Linköping Studies in Science and Technology

Dissertation No. 1295

Ultra-Wideband Low-Noise Amplifier and Six-Port Transceiver for High Speed Data Transmission

Adriana Serban

Department of Science and Technology

Linköping University, SE-601 74 Norrköping, Sweden

Norrköping 2010

Ultra-Wideband Low-Noise Amplifier and Six-Port Transceiver for High Speed Data Transmission

Adriana Serban

A dissertation submitted to the Institute of Technology, Linköping University, Sweden for the degree of Doctor of Technology.

Cover image: *Engineering – State-of-the-Art*

Picture by the author.
Chip from the time at Sicon AB.
Photography: Anders Ödmark

ISBN: 978-91-7393-463-3
ISSN 0345-7524

Linköping University
Department of Science and Technology

SE-601 74 Norrköping
Sweden

Printed by LiU-Tryck
Linköping, Sweden, 2010

ABSTRACT

Today's data rates in wired networks can reach 100 Gbit/s using optical fiber while data rates in wireless networks are much lower - tens of Mbit/s for 3G mobile communication and 480 Mbit/s for ultra-wideband (UWB) short range wireless communications. This difference in data rates can mainly be explained by the limited allowed frequency spectrum, the nature of the radio signal and the high requirements imposed on all hardware designed for high speed and wideband wireless communications. However, the demand on wireless commercial applications at competitive costs is growing. The first step in regulations allowing higher data rates for wireless communications was taken in 2002, when the Federal Communication Commission (FCC) in USA released unlicensed the 3.1-10.6 GHz frequency band restricting only the power level (maximum mean equivalent isotropic radiated power density of a UWB transmitter is -41.3 dBm/MHz) in the band 3.1-10.6 GHz. But Europe, Japan and recently China have put additional restrictions on the 3.1-4.8 GHz band. The restrictions address the problems that have raised from the coexistence and co-location of the UWB systems with other narrowband wireless systems. Thus, the 6-9 GHz band combined with an increased modulation order scheme is of large interest.

Operating at higher frequency and wider bandwidth than today's communication technologies, with the general task of maximizing the wireless data rate while keeping the power consumption low, requires new communication system solutions and new circuit design approaches. These new solutions also require understanding of many multi-disciplinary areas which until the recent past were not directly related: from classic analog circuit design to microwave design, from modulation techniques to radio system architecture.

In this thesis, new design techniques for wide bandwidth circuits above 3 GHz are presented. After focusing on ultra-wideband low-noise amplifier (UWB

LNA) design for low-power and low-cost applications, the practical implementation and measurement of a 3.1-4.8 GHz UWB LNA is addressed. Passive distributed components of microstrip transmission lines are intensively used and their contribution to the UWB LNA performance is studied. In order to verify the design methodology while extending it to the UWB radio front-end, the UWB LNA is integrated on the same substrate with a pre-selecting filter with the frequency multiplexing function. In this way, the concept of frequency-triplexed UWB front-end is demonstrated for the Mode 1 multi-band UWB bandwidth 3.1-4.8 GHz. Using the proposed receiver front-end topology, better receiver sensitivity and selective operation can be achieved.

The later part of the thesis investigates ultra-wideband 6-9 GHz receiver and transmitter front-end topologies for Gbit/s data rates and low power consumption. To capture the advantages offered by distributed passive components, both the transmitter and receiver use the six-port correlator as the core of a passive mixer. Modelling and design of the 6-9 GHz UWB front-end transceiver include different receiver topologies and different modulation schemes. Finally, the 7.5 GHz UWB transceiver front-end is implemented and evaluated. Measurement results confirm the large potential of the six-port UWB front-end to achieve multiple Gbit/s data rates. This may open for future solutions to meet the continuous challenge of modern communication systems: higher data rates at low power consumption and low cost.

ACKNOWLEDGEMENTS

I would like to express my gratitude to following people who have supported me in countless ways during the last years:

My supervisor, Professor Shaofang Gong, for his supports, guidance and for giving me the opportunity to work in his research group.

Professor Mats Fahlman for his wonderful advice.

My colleagues, Dr. Magnus Karlsson, Allan Huynh, Joakim Östh, Owais, Jing-Cheng Zhang and Pär Håkansson, for their cooperation in our various projects.

Dr. Jaap Haartsen and Dr. Peter Karlsson for interesting discussion and their feedback to my work.

Sony Ericsson Mobile Communications AB and Vinnova in Sweden are acknowledged for financial support of the study.

Sophie Lindesvik, Marie-Louise Gustafsson and Lise-Lotte Lönndahl Ragnar for taking care of all administrative issues with a smile on their faces.

Måns Östring, Amir Baranzahi and all my colleagues at ITN for their support, advice and friendship.

My friends, Anders Ödmark and Professor Mihai Datcu for encouraging me to take new challenges.

Last but not least, I would like to express my deepest gratitude to my beloved family with special thanks to my parents, my daughter Adina and her husband James, my wonderful husband Radu and my father-in-law Valeriu for their love, encouragement and support on short and long distance.

Adriana Serban
Linköping, February 2010

LIST OF PUBLICATIONS

Papers

I. Adriana Serban and Shaofang Gong**,** "Component Tolerance Effect on Ultra-Wideband Low-Noise Amplifier," *IEEE Transactions on Advanced Packaging* (accepted for publication).

II. Adriana Serban, Joakim Östh, Owais, Magnus Karlsson and Shaofang Gong, Jaap Haartsen and Peter Karlsson, "Six-Port Transceiver for 6-9 GHz Ultra-Wideband Systems," *Microwave and Optical Technology Letters* (accepted for publication).

III. Adriana Serban, Magnus Karlsson and Shaofang Gong, "A Frequency-Triplexed RF Front-End for Ultra-Wideband Systems," *ISAST Transactions on Electronics and Signal Processing*, No. 1, Vol. 2, pp. 83 - 88, 2008.

IV. Adriana Serban, Magnus Karlsson and Shaofang Gong, "Microstrip Bias Networks for Ultra-Wideband Systems," *ISAST Transactions on Electronics and Signal Processing*, No. 1, Vol. 2, pp. 16 - 20, 2008.

V. Adriana Serban, Magnus Karlsson and Shaofang Gong, "All-Microstrip Design of Three Multiplexed Antennas and LNA for UWB Systems," *Proceedings of the 2006 Asia-Pacific Microwave Conference*, Yokohama, Japan, December 2006, pp. 1109 – 1112.

VI. Shaofang Gong, Magnus Karlsson, Adriana Serban, Joakim Östh, Owais, Jaap Haartsen and Peter Karlsson, "Radio Architecture for Parallel Processing of Extremely High Speed Data," *Proceedings of the 2009 IEEE International Conference on Ultra-Wideband (ICUWB)*, Vancouver, Canada, September 2009.

VII. Adriana Serban, Joakim Östh, Owais, Magnus Karlsson, Shaofang Gong, Jaap Haartsen and Peter Karlsson, “Six-Port Direct Carrier Modulator at 7.5 GHz for Ultra-Wideband Applications,” manuscript.

Not included in this thesis:

VIII. Adriana Serban Craciunescu and Shaofang Gong, “Ultra-wideband Low-Noise Amplifier Design for 3.1-4.8 GHz,” in *Proc. GigaHertz 2005 Conference Uppsala*, Sweden, pp. 291 - 294, 2005.

IX. Adriana Serban Craciunescu and Shaofang Gong , “Low-Noise Amplifier Design at 5 GHz,” *The IMAPS Nordic Annual Conference, 2005*, pp. 227 – 229, Tønsberg, Norway, 2005.

X. Shaofang Gong, Magnus Karlsson, and Adriana Serban**,** “Design of a Radio Front-End at 5 GHz,” *Proceedings of the IEEE 6th Circuits and Systems Symposium on Emerging Technologies*, 2004, vol. I, pp. 241 - 244.

XI. S. Gong, A. Huynh, M. Karlsson, A. Serban, Owais, J. Östh, J. Haartsen and P. Karlsson, ” Truly Differential RF and Microwave Front-End Design”, accepted for presentation at *2010 IEEE WAMICON*, Melbourne, FL. USA.

XII. Adriana Serban, Joakim Östh, Owais, Magnus Karlsson, Shaofang Gong, Jaap Haartsen and Peter Karlsson, “Six-Port Direct Carrier Modulator at 7.5 GHz for Ultra-Wideband Applications,” accepted for presentation at *Gigahertz 2010 Symposium*, March 9-10, Lund, Sweden.

XIII. Joakim Östh, Adriana Serban, Owais, Magnus Karlsson, Shaofang Gong, Jaap Haartsen and Peter Karlsson, “Six-Port Gigabit Demodulator at 7.5 GHz for Ultra-Wideband Applications,” accepted for presentation at *Gigahertz 2010 Symposium*, March 9-10, Lund, Sweden.

LIST OF ABBREVIATIONS

ADS	Advance Design Systems
BiCMOS	Bipolar Complementary Metal-Oxide-Semiconductor
BPF	Band Pass Filter
CG	Common-Gate
CE	Common-Emitter
CMOS	Complementary Metal-Oxide-Semiconductor
CS	Common-Source
DAA	Detect And Avoid
dc	direct current
DSP	Digital Signal Processing
DSSS	Direct-Sequence Spread Spectrum
DS-UWB	Direct-Sequence Ultra-Wideband
DUT	Device Under Test
EDA	Electronic Design Automation
EDR	Enhanced Data Rate
EM	Electromagnetic
FET	Field-Effect Transistor
FMN	Frequency Multiplexing Network
FR-4	Flame Resistant 4
GSM	Global System for Mobile Communications
HBT	Heterojunction Bipolar Transistor

HiperLAN	High Performance Radio Local Area Network
IA	Instrumentation Amplifier
IC	Integrated Circuit
IEEE	Institute of Electrical and Electronic Engineers
IF	Intermediate Frequency
IIP3	Input-Referred Third-Order Intercept Point
I/Q	In-phase and Quadrature phase
ISM	Industrial, Scientific, Medical
ITN	Department of Science and Technology
LDC	Low Duty Cycle
LNA	Low-Noise Amplifier
LO	Local Oscillator
LPF	Low Pass Filter
LTE	Long Term Evolution
MBOA	Multiband OFDM Alliance
MIMO	Multiple-Input Multiple-Output
MMIC	Microwave Monolithic Integrated Circuit
Mbps	Mega bit per second
NF	Noise Figure
OFDM	Orthogonal Frequency-Division Multiplexing
QAM	Quadrature Amplitude Modulation
QPSK	Quadrature Phase Shift Keying
PCB	Printed Circuit Board
RADAR	Radio Detection And Ranging
RF	Radio Frequency
RO4350B	Rogers material 4350B
RX	Receiver

R&D	Research and Development
SiP	System-in-Package
SoC	System-on-Chip
SNR	Signal-to-Noise Ratio
S-Parameter	Scattering Parameter
SNR	Signal-to-Noise Ratio
TX	Transmitter
UWB	Ultra-Wideband
VCO	Voltage-Controlled Oscillator
VGA	Variable Gain Amplifier
VNA	Vector Network Analyzer
WLAN	Wireless Local Area Network
WPAN	Wireless Personal Area Network

CONTENTS

PART I

BACKGROUND

CHAPTER 1 INTRODUCTION

The technology of wireless transmission goes back to James Clerk Maxwell (1831-1879), a Scottish mathematician who in his work *Electricity and Magnetism*, published in 1873 predicted the existence of electromagnetic waves [1]-[2]. Maxwell unified a long series of previous discoveries, from Coulomb's law to Faraday's law, introducing the abstract concepts of *field* and *electromagnetic field* [2]. Already in 1864 he observed that "light itself is an electromagnetic disturbance in the form of waves propagated through the electromagnetic field according to electromagnetic laws" [3]. His theory not only prepared the way to Einstein's theories of relativity but also led to several revolutionary inventions which permitted long-distance communications between humans through the so called "vaccua": from the first electric telegraph in 1837, the first patented telephone in 1876, to the discovery of the radar (RAdio Detection And Ranging) in 1939.

The extraordinary development in the field of wireless transmission has been made possible also by the development in electronic components and microelectronics, resulting in complex circuits seamlessly processing radio signals with a large range of frequencies and modulation techniques. One of the first steps towards modern electronics was the invention of the silicon transistor in 1954 at Texas Instruments after the invention of the point-contact transistor by Bardeen, Brattain, and Shockley at Bell telephone laboratories in 1947. The subsequent development, the integrated circuits (ICs) made with silicon using the planar manufacturing process invented at Fairchild in 1958, has *closed* the circle opened by Maxwell more than 100 years ago while *opening* for a new era, the wireless era. Today, wireless communication is present everywhere enabling information to be exchanged around the world through high-capacity wireless links. Most of the technology surrounding us, our phones, computers, printers, cameras and TVs but also airplanes and satellites can be interconnected within

an invisible network. The freedom given us by the new possibilities to control and process electromagnetic waves has changed the way we communicate, our lives, and our way of thinking.

1.1. The Data Rate Challenge and Spectrum Implications

In the beginning, wireless communication technology was mostly used for military purposes. The breakthrough came only later when it became available firstly for broadcasting and then as mobile phones to the average consumer around the world. In a short time period, the common scientific and technological roots reaching back to Maxwell's theory [2] and Guglielmo Marconi's first radio transmission have developed into a global market and dynamic industry driven by an ever increasing number of applications with improving performance and functionality [4]. Taking one example, the first generation (1G) mobile phones from 1980s have evolved to the third generation (3G) phones that can handle not only calls but also e-mails, web surfing, music or stream video files. At the moment of writing this thesis, the world's first publicly available fourth generation (4G/LTE) service was opened in the two Scandinavian capitals, Stockholm and Oslo. The evolution towards wireless service diversity and better performance is reflected also in the increasing number of wireless standards. Figure 1.1 illustrates obviously that their entire evolution has a common driving force, i.e., the necessity of transmitting data faster.

In order to distinguish among the multitude of the existing standards, they can be here roughly divided into global-range standards and short-range standards. Global-range standards are cellular standards such as Global System for Mobile communication (GSM). Short-range standards, like Bluetooth, address mainly wireless data systems of short-range and high data rates. For global-range wireless cellular standards, the data rate has changed from several hundreds of kbit/s of the second generation (2G) devices to tens of Mbit/s of the third generation (3G) devices [5]. Even a more dramatically increase of the data rate can be noticed for the short-range wireless standards, represented in Figure 1.1 by Bluetooth, IEEE 802.11a/g and UWB. In the late 1990s, Bluetooth devices started to provide 1 megabit of data per second.

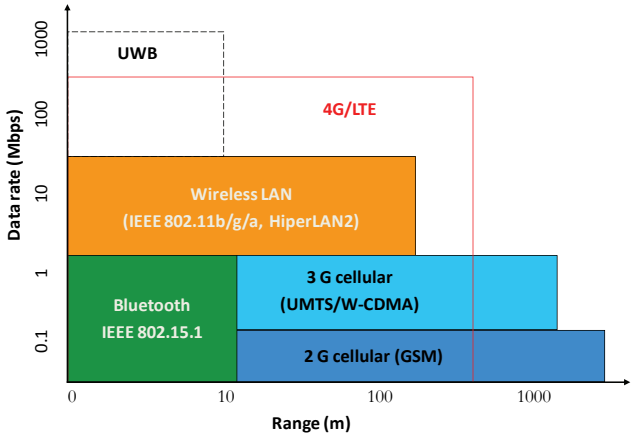

Figure 1.1 Wireless technologies and the data rate challenge.

The IEEE 802.11 (a/g) devices and corresponding wireless technologies have successively pushed the performance to 100 Mbit of data per second (100 Mbit/s) [6].

However, the highest expected data rate in Figure 1.1 corresponds to the ultra-wideband (UWB) technology, a relatively newly permitted method of using *a very large spectrum* with such a low-power that can co-exist with other licensed services. The UWB technology with access to 7.5 GHz bandwidth (3.1-10.6 GHz in USA) can provide data rates at least five times the data rate of the IEEE 802.11 standard at a short-range of 2 to 10 m and has the potential to become the core technology for wireless personal area networks (WPANs).

1.2. Short-Range Wireless Systems

Short-range communication systems have rapidly gained popularity in a wide range of application areas, including video and data transmission, wireless connections for personal computers, health care, home automation, security and general purpose sensing and monitoring.

Some of the main characteristics of the short-range communication systems are low-power consumption, radio range between several meters and several hundred meters, and principally indoor operation. A number of standards or regulations exist:

- IEEE 802.11a/b/g (Wi-Fi)

- HiperLAN2
- Bluetooth
- ZigBee, IEEE 802.15.4
- Ultra-Wideband (UWB)

IEEE 802.11 is a wireless local area network (WLAN) standard for different data rates. It was created in 1997 by the Institute of Electrical and Electronics Engineers (IEEE) and soon was extended to different specifications [7]:

- 802.11a operates in the 5 GHz band using orthogonal frequency-division multiplexing (OFDM). It has a maximum data rate of 54 Mbit/s.
- 802.11b was developed in parallel with 802.11a. It operates at 2.4 GHz band and uses direct-sequence spread spectrum systems (DSSS) to reach a data rate of 11 Mbit/s.
- 802.11g combines the 802.11a and 802.11b specifications. It operates in 2.4 GHz band using OFDM. The data rate is 54 Mbit/s.
- 802.11n is the newest specification for a 802.11 standard. It improves significantly the 802.11g by using the multiple-input multiple-output (MIMO) technique and provides about 300 Mbit/s data rate at 5 GHz.

HiperLAN (High Performance Radio Local Area Network) adopted by the European Telecommunication Standard Institute (ETSI) for WLAN is the European equivalent of 802.11a. It operates at 5 GHz [8].

Bluetooth is a low-cost, low-power technology, vastly utilized in wireless personal area networks (WPANs) [9]. Bluetooth is aimed to replace the cumbersome wire connections between different devices such as printer cables, headphone cables, wires between personal computers (PCs) and the keyboard or the mouse. It operates in the 2.4-GHz industrial, scientific and medical (ISM) band. Several classes exist with ranges between 10-100 m. The maximum data rate with EDR (Enhanced Data Rate) is 3 Mbit/s.

ZigBee (IEEE 802.15.4) is a low-cost, low-power technology for low-rate WPAN (LR-WPAN) and for wireless sensor networks (WSN) [10]. A ZigBee network is often a battery-powered, robust, self-configuring network. It operates in the 2.4 GHz spectrum. The peak data rate is 250 kbit/s.

Ultra-Wideband (UWB) Technology is a low-power technology firstly approved in USA for indoor wireless communication in the 3.1-10.6 GHz frequency band with a limited isotropically-radiated power (EIRP) of -41.3 dBm/MHz. UWB was intended from the beginning for short-range operation in WPAN. Combining a lower power and broader spectrum, it improves the speed and has the potential to avoid interference with other wireless systems [11]. The UWB technology is presented in more detail in the following section.

Moreover, as the frequency spectra below 10 GHz is expected to become crowded, there is now interest to build the 60 GHz radio technology. Recently, the WPAN standard 802.15.3 has defined an alternative physical layer (PHY) and a new millimeter-wave WPAN was approved, 803.15.3c [12]. The 60 GHz mm-wave communication system operates in the 57-64 GHz unlicensed band and it is planned to support at least 1 Gbit/s data rate applications, such as high speed internet access, video on demand, and HDTV.

1.3. UWB System Specifications

The potential of the UWB communication systems to achieve a high data rate can be explained by considering the Shannon's equation C = B log2(1+SNR), where C represents the data rate or channel capacity, B the available frequency bandwidth, and SNR signal-to-noise ratio. The SNR can be further expressed as SNR = PS/PN where PS is the average signal power and PN is the average noise power at the receiver and directly proportional to the bandwidth B. Since C depends stronger on B (linearly) than on SNR (logarithmical dependency with the SNR), the equation shows that the most effective way to get a higher data rate is by using a *larger bandwidth*.

Driven by increasing demand on short-range and high-data-rate wireless communications, the first step towards higher wireless data rates was taken in 2002, when the Federal Communication Commission (FCC) in USA released the unlicensed 3.1-10.6 GHz frequency band. According to the FCC rules, UWB devices would be required to have -10 dB fractional bandwidth of at least 0.20 or a -10 dB bandwidth of at least 500 MHz [13]. The power spectral energy (PSD) measured in a 1 MHz resolution bandwidth is restricted to -41.3 dBm.

In Europe, Asia and Japan additional restrictions in the form of LDC (Low Duty Cycle) and DAA (Detect and Avoid) to avoid interference with existing

narrowband systems have been put on the 3.1-4.8 GHz band. In Europe, the European Commission (EC) has detailed the UWB licensing regulations in 2007 for predominately in-door wireless applications. The EC has limited the UWB spectrum for UWB devices without requirements for DAA mitigation techniques to 6-8.5 GHz and -41.3 dBm/MHz [14]. In Japan, the national institute of information and communication (NICT) has allocated two frequency bands for UWB radio transmission: one from 3.4 to 4.8 GHz and the other from 7.25 to 10.25 GHz. However, only in the higher band, no interference mitigation techniques are necessary. The average transmission power is limited to -41.3 dBm/MHz in the higher band and to -70 dBm/MHz in the lower band [14]. In China, the bands 4.2-4.8 GHz and 6–9 GHz have been recently approved for UWB operation [16].

To date, the UWB regulatory extends through Asia, Europe and North America. From an industrial point of view, the telecom world including operators and handset manufacturers is very concerned about coexistence and co-location issues. To avoid interference with other radio systems, the 6-9 GHz band is preferred to be used for UWB. A graphical representation of the worldwide regulatory status is available at [17] and the co-existence of the UWB spectra with other standards is illustrated in Figure 1.2.

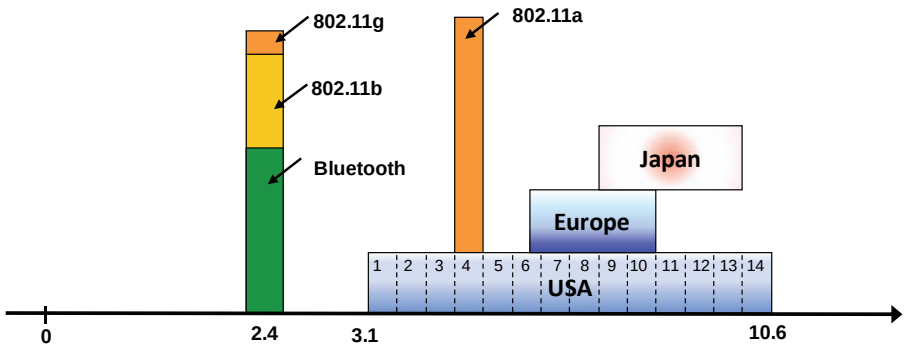

Figure 1.2. Worldwide UWB usable bands without protection requirements.

From the data transmission point of view, one general classification of the UWB systems is in (a) carrier-free UWB and (b) carrier-based UWB. In carrier-free UWB, also known as impulse-radio UWB, the signals are generated as short, shape-controlled pulses occupying the entire allocated band. Carrier-free communication systems are also called singleband systems. Carrier-based UWB can be implemented as single-carrier or as multi-carrier. Single-carrier UWB systems are based on spread spectrum (SS) techniques, which allow simultaneous use of a wide frequency band, as for example direct-sequence spread spectrum systems (DSSS). Multi-carrier systems use orthogonal frequency-division multiplexing (OFDM), a technique of transmitting data in parallel by using several modulated and orthogonal carriers [18].

Compared to the impulse radio UWB approach, which stems from work begun in the 1960s, the multiband UWB communication system with OFDM (MB-OFDM) is a more recent approach supported by the MB-OFDM Alliance (MBOA) since June 2003. According to the MBOA and WiMedia specifications [19], the UWB spectrum is divided into 14 channels, each with a bandwidth of 528 MHz, as illustrated in Figure 1.3. In the first half decade of 2000s, the so-called “Band Group 1” covering the spectrum from 3.1 to 4.8 GHz has gained large interest. However, in the last years as the LDC and DAA additional restrictions were adopted in Europe, China and Japan for the lower bands of the UWB spectrum, the interest has started to move towards the 6-9 GHz band.

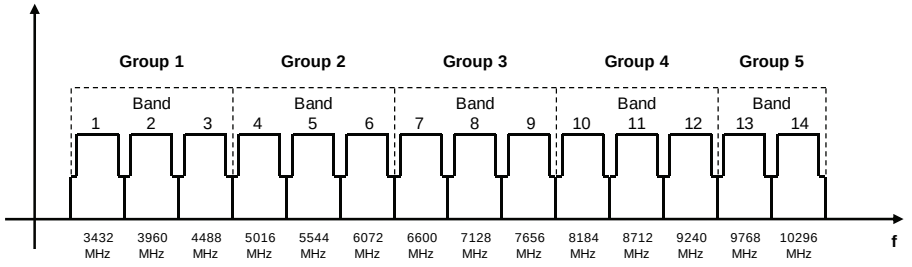

Figure 1.3. UWB multi-band proposal and band groups.

1.4. Summary and Trends

Wireless wideband communication systems for Gbit/s data rates, regulated or not by industrial communication standards, will continue to be in the center of research and development (R&D) activities in the future.

The best prospects are in the two ~7 GHz-wide bands at 3.1-10.6 GHz and 57-64 GHz.

Today's 60-GHz technology is based on power-hungry gallium-arsenide (GaAs) or silicon-germanium (SiGe) processes and have difficult to comply with the demand on low-cost and low-power devices [6]. Moreover, even if CMOS (Complementary Metal-Oxide-Semiconductor) processes could be used to implement 60 GHz transceivers in the future, at least the low-power goal seems difficult to achieve. Some of the drawbacks are the increased signal attenuation when propagating through the air, higher substrate losses due to ten times higher on-chip frequency and the necessary parallel architecture with several transceivers. However, it is interesting to notice that the GHz-wideband approach for short-range Gbit/s data rates wireless systems is so attractive that, despite huge technical challenges, a standard for the 57-64 GHz band has been recently approved as an extension of the WPAN standard IEEE 802.15.3, i.e., IEEE 802.15.3c [12].

In the 3.1-10.6 GHz band, at system, circuit, and device levels, challenges are not trivial for traditional transceiver for Gbit/s data rates. Among the technical difficulties, a few are listed:

- Broadband functionality at system and circuit levels.
- UWB low-noise amplifier (LNA), which for best performance requires broadband input and output matching networks.
- Generation of quadrature local oscillator (LO) signals at high frequency for modulation/demodulation operations in classical transmitter/receiver architectures.
- Passive on-chip components of high quality.
- Accurate components modeling over a large frequency band.

Due to its potential to achieve Gbit/s data rates [20] with lower power than wireless systems at 60 GHz, it is expected that research for multi-gigabit

wireless connectivity using UWB at 3.1-10.6 GHz will continue to be supported by R&D groups. Most probably, 3.1-10.6 GHz UWB and 60-GHz mm-wave radio will co-exist in different systems for different applications

Today, conventional transceiver architecture for UWB applications are narrowband solutions adapted to wideband operations by mainly using the enhanced computational power offered by the progress of CMOS IC technologies. Higher functional integration will continue to raise design complexity not only at the circuit and transistor levels, but also at the communication system level. However, on-chip solutions for high data rate transceiver imply parallel processing using complex algorithm to handle multi-level modulated signals at high frequency. This is in contradiction with the demand of low-power consumption.

Driven by the interest in high level of integration and low-cost mass fabrication, improvements are expected in the field of low-cost radio-frequency (RF) CMOS technologies, RF components and RF component modeling. However, the predicted aggressive scaling of CMOS transistors down to 16 nm in 2019 [21] may give huge benefits for digital circuits, but not in the same scale for RF circuits. The general trend is to reduce the analog processing of the RF signals within the front-end by shifting the analog/digital interface as close as possible towards the antenna. One reason why the analog processing is avoided is explained by the difficulty to implement analog high frequency circuits in ever better modern CMOS processes. Reduced supply voltage with technology scaling and the low quality factor of the inductors (Ls) are some of the drawbacks for the RF CMOS circuits. Generally, it is considered that passive components, on-chip capacitors and inductors of better precision and higher resonance frequencies will continue to be the bottle-neck for the on-chip front-end circuits [21].

One interesting possibility towards low-cost, low-power Gbit/s is represented by the UWB devices. Some challenges faced by present UWB front-ends integrated in standard CMOS processes derive from their circuit implementation and the traditional design methodology. Within the UWB band signals are voltage and current *waves*, best handled by microwave circuits. Hence, future UWB devices can be successfully implemented using unconventional receiver and transmitter front-ends which, on one hand do not ignore the wave nature of the UWB

signals, i.e., front-ends based on microwave circuits and on the other hand can adapt the microwave circuits to low-cost processes in form of system-in-package (SiP) intensively using distributed components.

Many studies were done in the past trying to investigate both the advantages and disadvantages of using lumped or distributed components, and on-board or on-chip inductors or matching networks. As we can see, these questions are not only still up-to-date but also even more critical since modern RF integrated circuit (IC) technologies cannot produce on-chip high-quality passive-components necessary for demanding low-power, high data-rate wireless-applications. In fact, lumped passive devices are not only a problem when they are integrated on chip, but also when they are mounted on circuit boards. In any mobile phone, GPS receiver, computer or other consumer electronics system, they dominate the area and limit the performance of modern high-frequency, broadband applications due to their parasitics. Moreover, they cannot be sized to any desired value, and their tolerances are still too high.

To integrate these passive components such as inductors, capacitors and matching networks, filters and antennas as a part of the board itself in form of miniaturized distributed components is one of the main challenges in the development of complete radio transceivers for wireless applications. Moreover, taking advantage of the microwave circuit state-of-the-art, other circuit within the transceiver chain can be successfully implemented using distributed components in low-power, low-cost printed circuit board (PCB) processes rather than on silicon. The optimal design solution will be in the future also a matter of defining the interface between what is the best of on-chip integration (SoC) and the best of package integration (SiP) [23].

1.5. Motivation and Scope of the Thesis

The future of above Gbit/s wireless products and services for the average consumer is dependent on the possibility to develop low-cost, low-power devices.

Given the limitations of the RF IC devices in terms of power consumption and cost, we have to reconsider our communication system architectures, circuit topologies and design methodologies. On the circuit and system level, the potential of microwave circuits based on distributed passive components to

process multi-level modulated signals at high frequency can be creatively exploited for future UWB applications. The idea in the beginning of the “world digitalization revolution” that passive components can be in the future totally avoided in ICs is now more and more replaced by the idea that new and improved passive components can contribute to communication circuits and innovative system solutions.

To answer these questions, UWB circuits and unconventional UWB front-end topologies for Gbit/s data rates have been investigated in this thesis. The first part of the thesis presents the low-noise amplifier (LNA) with multi-section distributed matching networks. In the second part, an unconventional 6-9 GHz six-port transceiver for Gbit/s data transmission is presented. The circuits were modeled, implemented in a low-cost printed circuit board (PCB), measured and conclusions are drawn.

The seven papers included in this thesis reflect the two main directions of the research:

In *Papers I, III, IV, V,* UWB low-noise amplifier design using multi-section distributed matching networks and 3.1-4.8 GHz UWB front-end topologies are presented. Related circuit designs are also considered, such as UWB bias networks design. *In Paper I,* the effect of passive component and manufacturing process tolerances on the low-noise amplifier performance is theoretically studied by means of sensitivity analysis. Simulation and measurement results are presented for verification of the analytical results. It is shown that, compared with a lumped matching network design, a microstrip matching network design significantly reduces the ultra-wideband low-noise amplifier sensitivity to component tolerances. In *Paper III* and *Paper V*, the concept of a 3.1-4.8 GHz multi-band UWB radio front-end consisting of three frequency multiplexed antennas and a low-noise amplifier (LNA) connected by a frequency multiplexing network (FMN) is presented. The proposed antenna-LNA system consists of three inverted-F antennas, and the UWB LNA. Introducing the frequency multiplexing network, one antenna for each sub-band and an LNA designed for maximum-flat power gain provides equal performance within the entire frequency band. In the LNA topology selection, design trade-offs such as low noise matching, high flat power gain, are discussed. The LNA employs dual-section input and output matching networks and is optimized for wideband

operation and minimum noise figure. The antennas, the frequency multiplexing network, the matching networks and the bias circuit of the LNA are all implemented using microstrip lines. Besides UWB LNA design, in *Paper IV* broadband bias networks with different radio frequency chokes were studied. It was shown that they can have different advantages in terms of bandwidth and occupied area. Drawbacks in terms of sharp discontinuities of the transfer functions in these types of bias networks were explained and the robustness of different bias networks against resonance was investigated. Different bias networks were fabricated and measured. Both simulation and experimental results show that broadband microstrip bias networks can be optimized to avoid or reduce the resonance phenomena. During this research, narrowband LNA for 5.25 GHz and UWB LNA for 3-5 GHz and 6-9 GHz based on microstrip matching networks were developed and manufactured. Advanced design techniques were used, for example electromagnetic (EM) simulations of the entire layout of the LNA module as well as EM simulations of the UWB bias networks implemented using different microstrip elements.

In *Paper II,* based on the manufactured six-port correlator and true component circuit designs, behavioral models of a 6-9 GHz transceiver and simulation set-ups for QPSK (quadrature phase shift keying), 16- and 64-QAM (quadrature amplitude modulation) modulation/demodulation applications were developed in Advanced Design System (ADS) from Agilent Technologies Inc. In *Paper II* and *Paper VII* the concept of six-port modulator with controllable impedance terminations implemented with a field-effect transistor (FET) in the linear operation region is introduced. The 7-8 GHz direct carrier six-port modulator was modeled, manufactured and measured. In *Paper VI,* radio architecture for parallel RF signal processing intensively using distributed microwave components such as a frequency multiplexing network and six-port correlator is presented. The radio architecture is aimed for achieving extremely high data rate above 10 Gbit/s with good phase linearity, amplitude balance and low noise figure in a very large bandwidth.

1.6. References

[1] J.C. Maxwell, *A Treatise on Electricity and Magnetism*, 3rd ed. New York, Dover, 1954.

[2] J.C. Rautio, “Maxwell's legacy,” *IEEE Microwave Magazine*, vol. 6, June 2005, pp. 46 – 53.

[3] J.C. Maxwell, “A dynamical theory of the electromagnetic field,” in Royal Soc. Trans., vol. CLV, Dec. 8, 1864. Repr. in *The Scientific Papers of James Maxwell*, 1890, New York: Dover, pp. 451 – 513.

[4] G. Staple, K. Werbach, “The end of spectrum scarcity,” *IEEE Spectrum*, vol. 41, Mar. 2004, pp.48 – 52.

[5] T. S. Rappaport, *Wireless Communications*, Prentice Hall Inc., 2009, Ch. 1.

[6] B. Razavi, “Gadgets Gab at 60 GHz,” *IEEE Spectrum*, vol. 45, Feb. 2008 pp. 46 - 58.

[7] IEEE website: http://grouper.ieee.org/groups/802/11/Reports/802.11_Timelines.htm.

[8] ETSI website, http://www.etsi.org.

[9] Bluetooth website: http://www.bluetooth.com/Bluetooth/Technology/Works/Compare/

[10] http://www.zigbee.org/

[11] http://www.intel.com/technology/comms/uwb/index.htm

[12] http://www.ieee802.org/15/pub/TG3c.html

[13] Federal Communication Commission (FCC) “Revision of Part 15 of the Commission’s Rules Regarding Ultra-Wideband Transmission Systems, First Report and Order,” ET Docket 98-153, Feb. 2002.

[14] Radio Spectrum Committee, ECC Decision of 1 December 2006 amended Cordoba, 31 October 2008, available at: http://ec.europa.eu/information_society/policy/ecomm/radio_spectrum/manage/eu/rsc/rsc_subsite/recent_meetings/index_en.htm.

[15] AWF3/14, “Technical Conditions on UWB Radio Systems in Japan,” MIC, Japan.

[16] http://www.wimedia.org/en/events/index.asp?id=events, 2009.

[17] http://www.wimedia.org/en/resources/worldwide_regulatory.asp, 2009.

[18] L. W. Couch, Digital and Analog Communication Systems, Prentice-Hall, 2001, Ch. 5.

[19] Multiband OFDM Physical Layer Specification, Release 1.1, MB-OFDM Alliance, WiMedia Alliance, Jul. 14, 2005.

[20] Shaofang Gong, Magnus Karlsson, Adriana Serban, Joakim Östh, Owais, Jaap Haartsen and Peter Karlsson, "Radio Architecture for Parallel Processing of Extremely High Speed Data," *2009 IEEE International Conference on Ultra-Wideband*, Sep. 2009, Vancouver, Canada. (*Paper VI*).

[21] http://www.itrs.net/Links/2008ITRS/Home2008.htm

[22] R. Ulrich, L.Schaper, "Putting passives in their place," *IEEE Spectrum*, vol. 40, Jul. 2003, pp. 26 – 30.

[23] "The next Step in Assembly and Packaging: System Level Integration in the package (SiP)," white paper at http://www.itrs.net/papers.html, 2009.

CHAPTER 2 ULTRA-WIDEBAND LOW-NOISE AMPLIFIER

This chapter investigates several low-noise amplifier (LNA) design aspects for ultra-wideband (UWB) systems with focus on UWB LNA design between 3.1-4.8 GHz. More details are to be found in *Papers I*, *III*, *IV* and *V*.

2.1. Introduction to Wideband Low-Noise Amplifiers

One of the most promising wideband technologies for short-range indoor data communication is the ultra-wideband technology. The UWB spectrum has been defined from 3.1 to 10.6 GHz by the Federal Communication Commission (FCC) [1]. A variety of UWB systems can be designed to use the 7.5 GHz spectrum. Among the existing architectural solutions, two of them have mainly contributed to intensive research and development (R&D). As shown in Chapter 1, one approach employs Orthogonal Frequency-Division Multiplexing (OFDM) in a multiband (MB) radio structure (MB-OFDM) [2], and the other is a singleband Direct-Sequence Spread Spectrum (DSSS) radio [3-4]. In the multiband approach the UWB spectrum is partitioned into several 528-MHz.

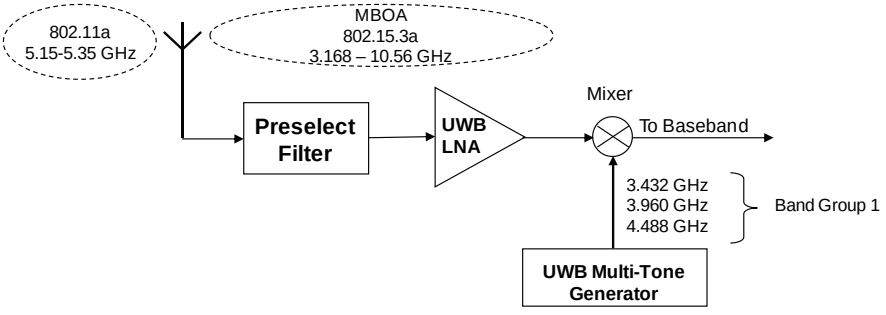

Figure 2.1 MBOA front-end block diagram.

bands and the so-called “Band Group 1” covers the spectrum from 3.1 to 4.8 GHz.

Regardless of whether it is an MB-OFDM system or a DSSS system, the UWB system must coexist with other narrowband wireless systems such as IEEE802.11a, as illustrated in Figure 2.1. The coexistence of the UWB systems with other narrowband wireless systems is possible because the regulated UWB emission levels are below the emission levels currently allowed for unintentional emissions, i.e., near to the noise floor of those receivers. The power level of a UWB transmitter (TX) is limited to -41 dBm/MHz. However, the UWB front-ends must be able handle strong, nearby interferes, which can desensitize the UWB receiver. Considering the MBOA approach, Table 2.1 shows that an UWB receiver requires better receiver sensitivity and lower noise figure than an IEEE 802.11a receiver. Moreover, as shown in Section 1.4 these improved design parameters must cover at least the bandwidth of 528 MHz [5].

2.2. Low-Noise Amplifier in the Receiver Chain

One of the most important parameters which characterize the communication system performance is the receiver sensitivity, i.e. the minimum input signal level that can be detected. Communication reliability and radio range depend directly on the smallest signal that a receiver can process.

Table 1.1 MBOA UWB and IEEE 802.11a Specifications [5]

	MBOA UWB	IEEE 802.11a
Sensitivity [dBm]	-73	-65
Data Rate [Mbit/s]	480	54
Channel Bandwidth [MHz]	528	20
Receiver Noise Figure [dB]	6-7 dB	12-14 dB

The minimum input signal depends on the bandwidth (B) of the system, the noise figure (F) of the receiver and the output signal-to-noise ratio (SNR_{out}) [6]:

$$Sensitivity = -174\,dBm + 10\log B + NF + SNR_{out} \tag{2.1}$$

where -174 dBm represents the noise power that the source resistance delivers to the receiver, assuming conjugate matching at the receiver input.

The noise figure is the noise metric showing how much the signal degrades when passing through a device and is defined as:

$$F = \frac{SNR_{in}}{SNR_{out}} \tag{2.2}$$

where SNR_{in} and SNR_{out} are the signal-to-noise ratios measured at the input and output, respectively. According to (2.1), noise limits the smallest signal that a receiver can process, and thus the receiver sensitivity.

The importance of the noise figure of an LNA in a receiver chain can be understood by considering the Friis equation [7]:

$$F_{tot} = 1 + (F_1 - 1) + \frac{F_2 - 1}{G_1} + \frac{F_3 - 1}{G_1 G_2} + \ldots \frac{F_i - 1}{G_1 G_2 .. G_{i-1}} + .. \frac{F_k - 1}{G_1 G_2 .. G_{k-1}} \tag{2.3}$$

where G_{i} and F_{i} represent the power gain the noise figure of each stage in the front-end, respectively. As shown in Figure 2.1, the first active circuit after the antenna is the low-noise amplifier.

The Friis equation shows that:

- The overall front-end noise figure F_{tot} is dominated by the noise figure of the first stage, F_1, i.e., the noise figure of the LNA.
- The gain of the LNA, G_1, reduces noise contribution of the subsequent circuits in the front-end.

The system performance depends on the performance of each individual block, but the relationship between system and individual circuit performances is not a simple one. Designing each circuit in the chain for the best possible noise figure, power gain and linearity does not automatically result in the best system performance. Optimizing of system parameters is inherently a process of trading-off among different parameters. However, considering the importance of the noise figure and gain of an LNA with respect to the receiver sensitivity, it is a common practice to design the LNA for the lowest noise figure and for maximum attainable gain.

2.3. LNA Design Methodologies

In order to optimize noise figure and gain of the LNA and to accurately predict the behavior of a real LNA, models are required. Amplifiers can be modeled in many ways. One of them is the two-port network model. Generally, the two-port network is a flexible representation for both active and passive circuits, at low or high frequencies. At low frequencies, lumped models use parameters such as *Z* (impedances), *Y* (admittances), *h* (hybrid) or *ABCD*. At high frequencies distributed models use *S*-parameters, i.e., transmission and reflection coefficients [8]. Moreover, the two-port model can be used to represent noisy circuits.

The main difference between low and high frequency amplifier designs originates from the amplifier specifications within the operation frequency band. The specification includes information about (a) the necessary amplifier characteristics, (b) the input signals to be amplified, and (c) source and load impedance. The specification differences at low and high frequencies are summarized in Table 2.2 in terms of required source and load impedances for optimum amplifier parameters. The power gain matching conditions at high frequencies shown in Table 2.2, i.e., $Z_S = Z_{in}^*$ and $Z_L = Z_{out}^*$ can briefly be explained by the maximum power transfer theorem [8]-[9]. This leads to the necessity of input and output matching networks, IMN and OMN, respectively, as shown in Figure 2.2, where Z_0 is the characteristic impedance of the system, and Z_{in}, Z_{out}, Z_S and Z_L are the input, the output, the source and the load impedances, respectively.

Table 2.2 . Input and output termination conditions of different amplifiers types at low- and high-frequencies.

Frequency	Input signal	Output signal	Input Condition	Output Condition
Low-frequcency f < 1 GHz	Voltage	Voltage	$Z_S = 0$, $Z_{in} = \infty$	$Z_{out} = 0$, $Z_L = \infty$
	Voltage	Current	$Z_S = 0$, $Z_{in} = \infty$	$Z_{out} = \infty$, $Z_L = 0$
	Current	Voltage	$Z_S = \infty$, $Z_{in} = 0$	$Z_{out} = 0$, $Z_L = \infty$
	Current	Current	$Z_S = \infty$, $Z_{in} = 0$	$Z_{out} = \infty$, $Z_L = 0$
High-frequcency f > 1 GHz	Power wave	Power wave	$Z_S = Z_{in}^*$ LNA: $Z_S = Z_{opt}$	$Z_L = Z_{out}^*$

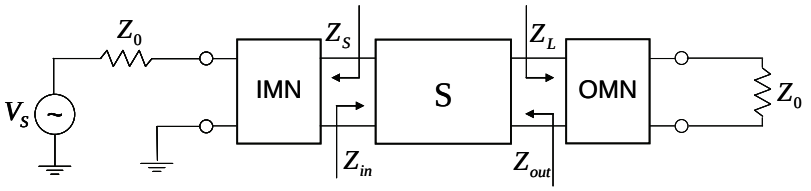

Figure 2.2 Generic two-port amplifier with input and output matching networks.

As shown in Table 2.2, the LNA design for minimizing the noise figure of an amplifier is given by $Z_S = Z_{opt}$.

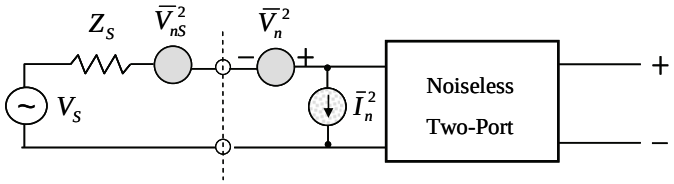

Figure 2.3 Two-port model for noise figure calculation.

This condition derives from the two-port model of a noisy network shown in Figure 2.3. Firstly, the internal noise sources of the network are transformed into equivalent input current and voltage noise sources, $\overline{I_n^2}$ and $\overline{V_n^2}$, respectively. Secondly, using $\overline{I_n^2}$ and $\overline{V_n^2}$, the noise figure of the network is expressed as a function of an optimum impedance [8]:

$$F = F_{\min} + \frac{G_n}{R_S}\left|Z_S - Z_{opt}\right|^2 \tag{2.4}$$

where F_{min} is the minimum noise factor that can be obtained when the source impedance Z_S is equal to an optimum impedance Z_{opt}. G_n is the equivalent noise conductance [8]. If Z_S is adjusted to Z_{opt}, the circuit yields the best achievable noise figure. If Z_S differs from Z_{opt}, the effect of the mismatch is amplified by G_n/R_S, where G_S and B_S are the source conductance and susceptance, respectively.

The history of the noise theory started in 1905 when Einstein explained the brownian motion of particles in fluids [10]. His mathematical model for random processes was then applied by Burgess [11] and Friis [12] to communication

systems and the noise figure was introduced as the parameter quantifying the noise properties in receivers. The noise figure minimization by mismatching impedances was demonstrated by Goldberg [13].

In general, high-frequency amplifier design can be done by using the lumped or distributed element method, as illustrated in Figure 2.4. For the same specification and amplifier topology, the two methods will come to the same conclusion [7]. In the lumped method at the circuit level, the design methodology is based on electrical parameters of the transistor and its small-signal equivalent model. Gain and stability analyses are performed for a specific amplifier topology using Bode diagrams. Noise analysis is performed using input equivalent voltage and current noise sources. Voltage and current are the primary variables of interest, while *Z*-, *Y*-, *h*- or *ABCD*-parameters describe the two-port model of the amplifier. In the distributed design method, the design methodology takes the distributed nature of the circuits into consideration. The analysis of the circuits is based on S-parameters.

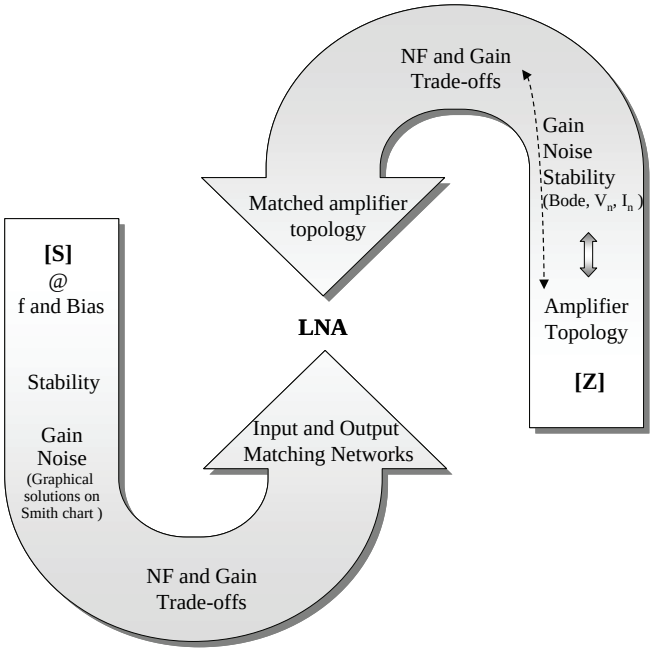

Figure 2.4. Distributed and lumped parameter design-flow.

Throughout the whole design process and at all hierarchical levels, active and passive circuits are treated as two-port networks with S-parameter representations, between input and output terminations. Gain and noise analyses result in graphical solutions on the Smith chart. The associated metrics representing stability, power gain and noise figure are described in terms of *S*-parameters. In both methods the complex conjugate impedance conditions must be fulfilled at the input and output interfaces in order to get the maximum power amplification or the minimum noise figure [7]-[8]. Stability is a primary design objective for all circuits, particularly for RF and microwave circuits.

2.4. Ultra-wideband low-noise amplifier design

In this thesis, the approach of ultra-wideband low-noise amplifier (UWB LNA) with multi-section input and output microstrip matching networks has been investigated. UWB LNAs with a low noise figure and a flat power gain have been implemented on a conventional printed circuit board and measured. Besides UWB LNA design, the effect of passive component and manufacturing process tolerances on the low-noise amplifier performance have been theoretically studied by means of sensitivity analyses and experimentally verified.

2.4.1. Wideband Matching Trade-Offs

The design of wideband matching networks is a network synthesis process, known as the “approximation problem” [14]. Given a resistive generator impedance Z_S and a frequency dependent load impedance Z_L, a reactive two-port network must be designed in order to achieve the prescribed constant power gain value over the specified frequency range. The conjugate impedance matching conditions are $Z_S = Z_{in}^*$ and $Z_L = Z_{out}^*$, see Figure 2.5a. Ideally, these conditions should be satisfied over the entire bandwidth $BW = \omega_2 - \omega_1$. The center frequency is defined as $\omega_0 = \omega_1 + (\omega_2 - \omega_1)/2$, where ω_1 and ω_2 are the lower and upper stop frequencies, respectively.

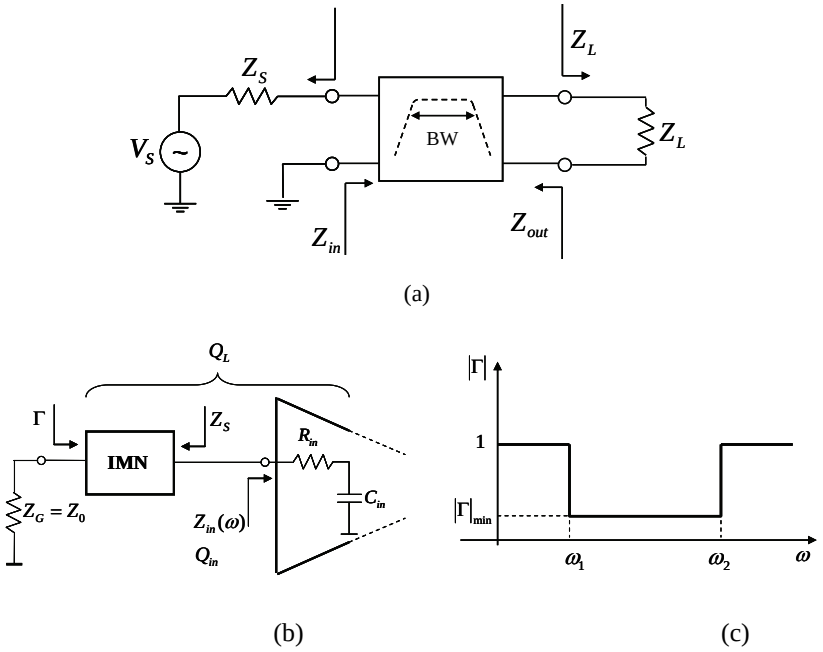

Figure 2.5. Matching networks for gain-bandwidth trade-offs [18].

The gain-bandwidth restrictions for lossless wideband matching networks were formulated by Fano [15]. Applying them to the amplifier design as shown in Figure 2.5b, they become:

$$\int_{\omega_1}^{\omega_2} \ln\left|\frac{1}{\Gamma}\right| d\omega \le \frac{\pi}{R_{in}C_{in}} \tag{2.5}$$

$$\left|\Gamma\right|_{\min} = e^{-\pi(Q_L/Q_{in})} = e^{-(\pi\omega_0)/(BW\times Q_{in})} \tag{2.6}$$

$$Q_{in} = \frac{1}{\omega_0 R_{in} C_{in}} \tag{2.7}$$

$$Q_L = \frac{\omega_0}{\omega_2 - \omega_1} = \frac{\omega_0}{BW} \tag{2.8}$$

where Q_{in} is the quality factor (Q-factor) of the equivalent small-signal input circuit of the amplifier and Q_{L} is the loaded Q-factor of the input matching network. The equivalent small-signal depicted input circuit of the amplifier is depicted in Figure 2.5b as an equivalent input resistor and capacitor, R_{in} and C_{in} in series. Equations (2.5-2.8) show that, the IMN can be implemented over a defined bandwidth (BW) only at the expense of less power transfer, or in terms

of reflection coefficient that $\Gamma \neq 0$ within the BW. Thus losses are inevitable for a given BW. From (2.6), for a small reflection coefficient, the loaded quality factor must be high, while from (2.8) the fractional bandwidth BW/ω_0 becomes smaller, when the quality factor increases.

Extrapolating the necessary and sufficient conditions of the wideband matching network theory to the design of the input matching network of UWB LNA, the following conclusions can be drawn:

- The minimum noise impedance matching conditions $Z_S(\omega) = Z_{opt}(\omega)$ at the input port of a UWB LNA cannot be maintained over the entire bandwidth. Noise figure values larger than F_{min} must be accepted.
- Noise figure of UWB LNAs can be optimized towards near-to-minimum values over a wide bandwidth when an input matching network of a low loaded quality factor is used.

2.4.2. Wideband Low-Noise Amplifier Design Techniques

Equation (2.4) shows that the minimum noise figure can be achieved when the source impedance $Z_S(\omega)$ is equal to the optimum noise impedance, i.e., $Z_S(\omega) = Z_{opt}(\omega) = R_{opt}(\omega) + jX_{opt}(\omega)$, where R_{opt} and X_{opt} are the resistive and the reactive parts of the optimum source impedance Z_{opt} required for the optimum noise figure. For narrowband LNAs, the noise matching condition is generally solved by a reactive single-section input matching network which presents the correct impedance only around the resonance frequency ω_0, in a bandwidth $BW_{-3dB} = \omega_0/Q$, where Q is the loaded Q-factor of the input matching network (noise figure-bandwidth trade-off). Owing to the inherent difference between Z_{opt} and Z^*_{in}, where Z^*_{in} is the complex conjugate of the transistor input impedance ($Z_{in} = R_{in}(\omega) + jX_{in}(\omega)$, where R_{in} and X_{in} are the resistive and the reactive parts of the input impedance Z_{in}), in an LNA design some power gain loss at the input is acceptable for a low noise figure of the amplifier (noise figure-power gain trade-off).

The UWB LNA design trade-offs are similar to those for narrowband LNA, but they are more difficult to satisfy. The key issue in UWB LNA design is the input and output impedance matching over a wide bandwidth: 3.1 to 4.8 GHz for the Mode 1 UWB band or 3.1 to 10.6 GHz for the entire UWB band. Classical amplifier design techniques which can be extended to the UWB-compliant LNA

design are: (a) amplifiers employing resistive shunt feedback [16]-[17] and (b) amplifiers employing multi-section input and output matching networks [18]-[19], conceptually shown in Figures 2.5a and 2.5b, respectively.

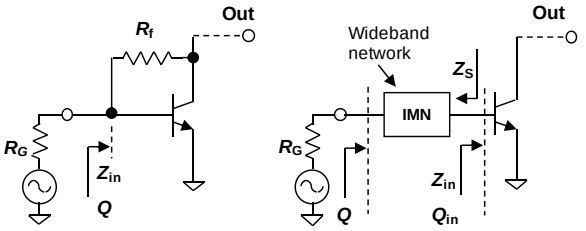

(a) (b)

Figure 2.5. Conceptual schematics of wideband amplifier topologies. (a) Resistive shunt feedback amplifier. (b) Wideband (multi-section) matching network amplifier. IMN = input matching network.

At high frequencies, their wideband properties can be explained considering that in both configurations the loaded *Q*-factor Q as defined in Figure 2.5 is lowered and, consequently, the -3-dB bandwidth is increased ($BW_{\text{-3dB}} = \omega_0/Q$). For the feedback amplifier shown in Figure 2.5a, the feedback resistor R_f reduces the *Q*-factor of the series equivalent input circuit by adding a supplementary resistive contribution, so that $R_{in,f} = R_{in} + \Delta R$ results in lower *Q*-factor value of the input circuit ($Q = 1/\omega_0 R_{in,f} C_{in}$). This technique, however, generally results in LNA designs with poor noise figure, low power gain and increased power consumption [16].

In the second amplifier topology shown in Figure 2.5b lossless matching networks (the output matching network is not shown) are synthesized [18] so that conjugate matching at the input of the active device will satisfy either the maximum power transfer condition ($Z_S = Z^*_{in}$) or the minimum noise figure condition ($Z_S = Z_{opt}$). Considering the input matching condition in Figure 2.5b, for the given ratio between the generator resistance R_G and the transistor input resistance R_{in}, and a single-section (L-network) matching network, the loaded Q-factor value of the matching network, $Q = Q_I$ is predetermined [20]-[22] and given by

$$Q_I = \sqrt{\frac{R_G}{R_{in}} - 1}; \quad \mathrm{R_G} > R_{in} \tag{2.9}$$

Usually, (2.9) results in matching networks of high loaded *Q*-values, i.e., narrowband matching networks.

For wideband impedance matching networks, two or more L-networks can be cascaded resulting in different filter topologies, e.g., *LC*-ladder filter topologies as shown in Figures 2.6a and 2.6b, or Chebyshev filter topologies [16].

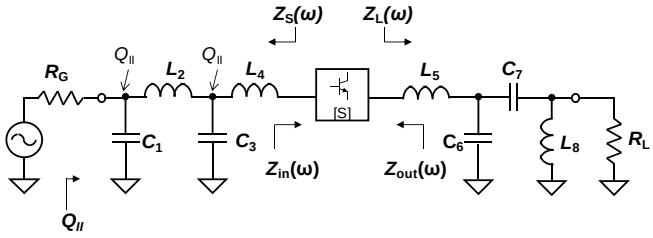

(a)

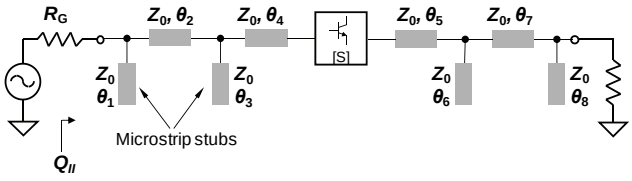

(b)

Figure 2.6. Multi-section UWB LNA topologies with (a) lumped and (b) distributed matching networks. Q_{II} is the loaded Q-factor

For a dual L-section lossless matching network of alternating (inductive, capacitive) passive components and bandwidth-optimal down-scaling from R_G to $R_S = R_{in}$, the loaded *Q*-factor value of the matching network $Q = Q_{II}$ is

$$Q_{II} = \sqrt{\sqrt{\frac{R_G}{R_{in}}} - 1}; \quad \mathrm{R_G} > R_{in} \tag{2.10}$$

With lower value of the Q-factor given by (2.10), the optimal input matching condition is achieved over a wide bandwidth without increase in power consumption.

2.4.3. Multi-Section Matching Network UWB Low-Noise Amplifier Design

Due to its design flexibility for optimal LNA parameters and the expected lower power consumption compared with the feedback topology, our proposed UWB LNA topology is the multi-section LNA. The UWB LNA was firstly analyzed for a 3.1–4.8 GHz UWB LNA.

In *Paper VIII*, various multi-section matching network topologies resulting in low-pass and band-pass power gain transfer characteristic were studied. The design focuses on the 3.1-4.8 GHz UWB LNA with multi-section distributed matching networks. Besides the desired frequency bandwidth, using dual-section matching networks, the *equalization* of the noise figure and power gain over the frequency band is demonstrated. Generally, the noise figure of amplifiers increases with frequency [8]. Designing the IMN such that $Z_S = Z_{opt}$ at an upper frequency of the LNA passband, and accepting larger mismatches at lower frequencies may result in constant noise figure over the entire frequency band. Figure 2.7 illustrates the equalization effect of the IMN over the noise figure characteristic [23].

As the IMN is used for achieving a close-to-minimum noise figure, the output matching network in a UWB LNA amplifier and in any UWB amplifier can be used to compensate for active device gain roll-off with frequency. With a dual-section OMN, flat power gain over the specified frequency band can be obtained if the OMN is designed such that $Z_L = Z_{out}^*$ at an upper frequency of the LNA passband, and thus accepting mismatches at lower frequencies.

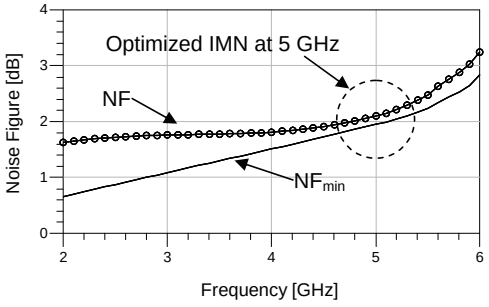

Figure 2.7 Constant noise figure design. Simulated noise figure of a UWB LNA using ADS [24]. Output noise figure (circles) and the minimum noise figure (solid line).

Figure 2.8 illustrates the equalization effect of the OMN over the power gain characteristics.

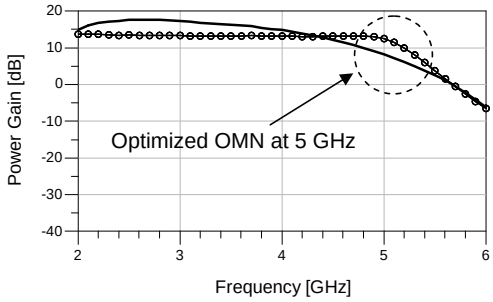

Figure 2.8 Simulated power gain of a UWB LNA using ADS [24]. Amplifier power gain when OMN is used (circles). Amplifier power gain when OMN is not used (solid line).

The design methodology was verified by implementing the 3.1-4.8 GHz UWB LNA in a frequency-triplexed RF front-end for Band Group 1. Presented in *Paper III* [25] and *Paper V* [26], the proposed solution combines a multi-band pre-selecting filter function with the frequency multiplexing function to connect three different RF inputs to only one 3.1-4.8 GHz LNA. The LNA UWB is optimized for a near-to-minimum noise figure and flat gain response The performed measurements have confirmed the LNA topology selection and the design methodology. They have also shown that our approach of using distributed components on a printed circuit board can result in complex front-end topologies for multi-band UWB applications characterized by low noise figure, low-power consumption and relatively small and controllable losses.

To complete the UWB LNA design aspects, the problem of bias-network design for typical UWB applications has been explicitly addressed in *Paper IV* [27]. The bias network of the LNA, is an optimized broadband bias network using the butterfly radial stub. Using simulation and measured results, it is shown that the butterfly stub is best suited for broadband RF choke applications. The RF choke using the butterfly stub gives not only the broadest band characteristic but also the most robust bias network towards (a) different layout geometries connecting the RF choke to the dc port, and (b) load impedance variation of the dc port.

2.5. Multi-Section Matching Networks: Distributed versus Lumped

The proposed technique to enhance the bandwidth of the LNA by using multi-section matching networks has several potential disadvantages, mainly because of the increased number of reactive passive components. Depending on passive component integration technologies, two different types of matching networks can be distinguished: (a) on-chip matching networks and (b) off-chip matching networks. For lumped passive components integrated in silicon, the major difficulty arises from substantial losses in inductors at frequencies above a few Giga-Hertz, resulting in an increased noise figure [28]. Other disadvantages are enlarged chip size, increased circuit complexity, large variations from the nominal value and the lack of accurate models over a large frequency range [29]-[30]. The need for high-performance on-chip passive components also results in additional photolithography and other process steps or new material included into existing processes. This makes lumped passive components on silicon, especially inductors, very costly. For the off-chip lumped passive components, the problem of tolerances and component modeling becomes critical above Giga-Hertz. In addition to their dimensions, which have decreased substantially for surface-mounted devices, lumped passive components can experience significant statistical uncertainty of their nominal values, typical values being ±10% to ±20% for capacitors, and even more, up to ±30%, for inductors [31]-[32] in the pF and nH range.

As known, other possible off-chip passive components are those integrated in the form of distributed components, e.g., microstrip transmission lines, in the existing printed circuit board of radio frequency (RF) modules. Since organic substrates of printed circuit boards are the most cost-effective solution for RF circuits today, they might be an interesting solution for a wide variety of circuits requiring low cost, low power consumption, high data rates and low noise figure [33]-[34].

In order to get a clear picture of how manufacturing tolerances affect RF circuit performance, in *Paper I* the sensitivity of UWB LNA implemented with distributed multi-section matching networks was investigated. Process and material tolerances with regard to the height (h) and dielectric constant (ε_r) of the

substrate, width and length (l) of the transmission lines (*w*) represented in Figure 2.9 are considered in simulations and measurements.

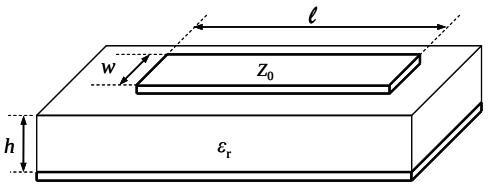

Figure 2.9 Microstrip transmission line represented by characteristic impedance (Z_0), width (w) and length (l). Printed circuit board represented by dielectric constant (ε_r) and height (h).

The presented theoretical study – for more details, see *Paper I* - simulation and measurement results have shown that the design of wideband LNAs with multi-section impedance matching networks is a good approach in terms of low noise figure, high power gain and wide bandwidth for any wideband amplifier supporting UWB or multi-standard wireless radio applications [6]-[7], [13]-[14].

Firstly, it was demonstrated that the dual-section UWB LNA performance is affected by the cumulative effect of passive component tolerances on the noise matching condition. It was also shown that lower LNA sensitivity can be achieved only by the use of high-precision passive components. Simulations have shown large deviations from the target value of the noise figure when the dual-section UWB LNA was implemented with lumped matching networks. However, simulation and measurement results of the UWB LNA implemented with distributed microstrip matching networks showed a very robust performance, despite the ±10% variation of the line width. This indicates that separate integration of distributed passive components in printed circuit board is a better alternative to both on-chip and off-chip lumped passive components.

The main disadvantage of the presented UWB LNA design is the occupied area. However, the size can be optimized both at UWB LNA level (better layout of the bias network and matching networks) and system level (antenna-LNA co-design on multi-layer substrates). The main advantages of the presented UWB LNA design using distributed microstrip matching networks are summarized as follows:

- The matching networks using microstrips are almost insensitive to typical printed circuit board manufacturing process tolerance. Through the use of microstrip transmission lines instead of on-chip and off-chip lumped passive components, the traditional problem of radio frequency integrated circuits, i.e., poor yield and high-cost, is thus avoided. Moreover, the distributed matching networks integrated in printed circuit board do not require any additional assembly process. In contrast, when lumped components are integrated into silicon integrated circuits or as off-chip discrete surface mounted devices, additional technology or assembly steps are needed.
- Electromagnetic simulations based on the matching network layout and the S-parameters of the transistor allow accurate optimization of the amplifier parameters, including all parasitic effects. In this way, the problem of inaccurate modeling of passive components over a large frequency spectrum is avoided.
- The distributed matching networks are closely integrated with the transistor. As shown in Figure 2.10, the advantages of flip-chip bonding techniques are such that a smooth transition between the transistor and the matching networks on the printed circuit board is realized, reducing the need for signals to propagate through any package.
- Since the passive components are integrated on the printed circuit board, the same active transistor or chip can be used with different passive components to achieve different amplifier or system performances.

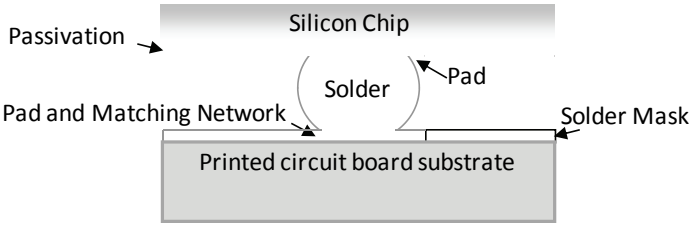

Figure 2.10. Illustration of flip-chip interconnection to the microstrip matching network on the printed circuit board.

2.6. UWB LNA Design – Summary

The LNA design must handle trade-offs such as LNA topology selection, wideband noise figure matching, flat power gain and wideband bias aspects. Optimally, UWB LNA design methodologies should provide improved receiver sensitivity and thus accurate low-level signal processing. In order to circumvent losses and thus minimize the noise figure of the front-end, the antenna or antenna-system should also be closely integrated with the LNA, preferably on the same RF module.

Generally, radio frequency circuit performances, unlike *digital* CMOS circuit performances, are mainly determined by passive elements. As shown in Section 2.4.2 the main trade-off between noise figure and power gain for a specified bandwidth can be solved by using a few amplifier topologies in conjunction with (a) wideband matching networks techniques and (b) resistive shunt feedback. In Appendix A, the main UWB LNA topologies implemented in CMOS technologies are briefly listed. Far from being an exhaustive listing of all UWB LNA designs, it offers a better insight of the necessary trade-offs and limitations that are specific for UWB LNA and UWB receiver design. As wideband amplifier topologies make use of a relatively large number of passive components, the main difficulty arises in achieving critical parameters for UWB LNA (near-to-minimum noise figure and flat power gain over the entire bandwidth) which are also less sensitive to passive component tolerances.

There are three main options for including passives into radio frequency circuits: (a) integration of passive components directly into the radio frequency integrated circuits, (b) assembling them as off-chip discrete components using a standard surface-mount technology, and (c) integrating them as distributed components using microstrips on the printed circuit board, as investigated in this work.

A hot topic today for radio frequency circuit design is system-on-chip, i.e., all the passive and active components are designed as a single integrated circuit, resulting in the most compact solution. However, as the passive components do not scale down following the Moore’s law, more passive components integrated into system-on-chip can result in a cost-ineffective solution in terms of enlarged chip area. In addition, the lack of accurate models of passive component and the problem of passive component tolerances lower the manufacturing yield. Consequently, passive component integration becomes a bottleneck in many

system-on-chip designs. In a consecutive reports, the International Technology Roadmap for Semiconductors (ITRS) identifies passive components as one of the critical challenges of future RF integrated circuits and recommends hybrid solutions based on off-chip passive components, i.e., passives separately integrated in different substrates or packages [35].

From our previous RF circuit designs, i.e., antenna [36]-[37], frequency-triplexer [38], narrowband and ultra-wideband LNAs [39]-[40], as well as considering the analysis and measurement results presented in *Paper I*, *III* and *V*, one important conclusion can be drawn: UWB circuits using distributed components of microstrips result in predictable and stable impedance values, near to the designed values.

The use of distributed microstrip matching networks is a well-known technique for monolithic microwave integrated circuits (MMICs) based on III–V semiconductors. However, this is still an expensive technology. In our research, it is shown that distributed matching networks can be successfully exploited using a conventional and low-cost printed circuit board technology.

Ultra-wideband low-noise amplifiers are expected also in the future to be the key component in the RF front-end of low-cost, high data rates radio systems for wireless communication. As SoC technology offers the promise for the most compact and low-cost radio system, designers around the world will continue to search the best way to integrate the entire radio system on the same silicon substrate.

However, as presented in this thesis, there are already some fundamental limits to accurate analog signal processing when the entire RF front-end of a UWB system must be integrated on the same chip. These limitations indicate that the future of successful RF front-end design in general, and of the UWB LNA design in particular, belong to a mixed, flexible radio system solution based on the best of on-chip integration and the best of package integration. Synergy effects resulting from merging the progresses of SoC and SiP or system-on-package (SoP) technologies will overcome the fundamental limits of SoC, while changing the conventional architecture and design methodologies of the RF front-end for Gbit/s applications.

2.7. References

[1] Federal Communication Commission (FCC) “Revision of Part 15 of the Commission’s Rules Regarding Ultra-Wideband Transmission Systems, First Report and Order,” ET Docket 98 - 153, Feb. 2002.

[2] P. Heydari, “A Study of Low-Power Ultra Wideband Radio Transceiver Architectures,” Proceedings of Wireless Communications and Networking Conference, 2005, pp. 758 – 763, vol. 2, Mar. 2005

[3] M. Z. Win and R. A. Scholtz, “Ultra-Wide Bandwidth Time-Hopping Spread-Spectrum Impulse Radio for Wireless Multiple-Access Communications,” IEEE Transactions on Communications, vol. 48, pp. 679 - 691, Apr. 2000.

[4] E. Fujita http//grouper.ieee.org/802/15/pub/2003/May03/03138r2P802-15.

[5] B. Razavi, T. Aytur, C. Lam, F. R. Yang, K. Y. Li, R. H. Yan, H. C. Hang, C. C. Hsu, C. C. Lee, “A UWB CMOS Transceiver,” *IEEE Journal of Solid-State Circuits*, vol. 40, no. 12, pp. 2555 - 2562, Dec. 2005.

[6] B. Razavi, *RF Microelectronics*, *Prentice Hall 1998*.

[7] B. Leung, “VLSI for Wireless Communication”, Prentice Hall 2002.

[8] R. Ludwig and P. Bretchko, *RF Circuit Design. Theory and Applications*, Prentice Hall 2000.

[9] T. H. Lee, *RF Circuit Design. The Design of CMOS Radio-Frequency Integrated Circuits*, Cambridge University Press 1998.

[10] A. Einstein, “Zur Theorie der Brownschen Bewegung,” Annalen der Physik, vol. 19, pp. 371 – 381, 1906.

[11] R. E. Burghes, “Noise in Receiving Aerial Systems,” Proceedings of the Physical Society, vol. 53, pp. 293 - 304, 1941.

[12] H. T. Friis, “Noise Figure of Radio Receiver” *Proceedings of the IRE*, vol. 32, pp. 419 – 422, 1944.

[13] H. Goldberg, “Some Notes on Noise Figure,” *Proceedings of the IRE*, vol. 36, pp. 1205, 1948.

[14] J. D. Mellor and G. J. Linvill, "Synthesis of Interstage Networks of Prescribed Gain Versus Frequency Slope," *IEEE Transactions on Microwave Theory and Techniques*, vol. 23, no. 12, pp. 1013 - 1020, Dec. 1975.

[15] R. M. Fano, "Theoretical Limitations on the Broadband Matching of Arbitrary Impedances," Journal of Franklin Institute, Jan. 1950.

[16] C.-W. Kim, M.-S. Kang, P. T. Anh, H.-T. Kim and S.-G. Lee, "An ultra-wideband CMOS low-noise amplifier for 3-5-GHz UWB system," *IEEE J. of Solid-State Circuits*, vol. 40, issue 2, pp. 544-547, Feb. 2005.

[17] 15 J. C. Zhan and S. S. Taylor, "A 5 GHz resistive-feedback CMOS LNA for low-cost multi-standard applications," in *IEEE Int. Solid-State Circuits Conf. Tech. Dig*., San Francisco, CA, Feb. 5-9, 2006, pp. 200 - 201.

[18] 16 A. Bevilacqua and A. M. Niknejad, "An ultrawideband CMOS low-noise amplifier for 3.1-10.6 GHz wireless receiver," *IEEE J. Solid-State Circuits*, vol. 39, issue 12, pp. 2259 - 2268, Dec. 2004.

[19] A. Ismail and A. Abidi, "A 3-10 GHz low-noise amplifier with wideband LC-ladder matching network," *IEEE J. Solid-State Circuits*, vol. 39, issue 12, pp. 2269 - 2277, Dec. 2004.

[20] G. Gonzalez, *Microwave Transistor Amplifier Analysis and Design*, Prentice-Hall, Upper Saddle River, New Jersey, 1997, pp. 344 - 352.

[21] T. H. Lee, *RF Circuit Design. The Design of CMOS Radio-Frequency Integrated Circuits*, second edition, Cambridge University Press, 2004, pp. 92 - 93.

[22] L. Besser and R. Gilmore, *Practical RF Circuit Design for Modern Wireless Systems*, Artech House, 2003.

[23] A. Serban and S. Gong, "Ultra-wideband Low-Noise Amplifier Design for 3.1 - 4.8 GHz" *GigaHertz 2005*, Uppsala, Sweden, pp. 291 - 294, Nov. 2005.

[24] Agilent Technologies Inc., "Advanced Design System (ADS)," http://eesof.tm.agilent.com/.

[25] Adriana Serban, Magnus Karlsson and Shaofang Gong, "A Frequency-Triplexed RF Front-End for Ultra-Wideband Systems," *ISAST Transactions on Electronics and Signal Processing*, No. 1, Vol. 2, pp.83 - 88, 2008.

[26] A. Serban, M. Karlsson and S. Gong, "All-Microstrip Design of Three Multiplexed Antennas and LNA for UWB Systems" *Asia-Pacific Microwave Conference (APMC) 2006*, Yokohama, Japan, December 2006.

[27] Adriana Serban, Magnus Karlsson and Shaofang Gong, "A Microstrip Bias Networks for Ultra-Wideband Systems," *ISAST Transactions on Electronics and Signal Processing*, No. 1, Vol. 2, pp. 16 - 20, 2008.

[28] J. N. Burghartz and B. Rejaei, "On the design of RF spiral inductors on silicon," *IEEE Trans. Electron Devices*, vol. 50, issue 3, pp. 718 – 729, Mar. 2003.

[29] B. Razavi, "Prospects of CMOS technology for high-speed optical communication circuits," *IEEE J. of Solid-State Circuits*, vol. 37, issue 9, pp. 1135 – 1145, Sep. 2002.

[30] T. S. D. Cheung and J. R. Long, "Shielded passive devices for silicon-based monolithic microwave and millimeter-wave integrated circuits," *IEEE J. of Solid-State Circuits*, vol. 41, issue 5, pp. 1183-1200, May 2006.

[31] Toko, *Chip inductors product catalog*. Available: www.toko.com. Selection Guide: Chip inductor type: LL1005FHL.

[32] Murata, *Chip monolithic ceramic capacitors product catalog*. Available: www.murata.com. Capacitors type: GJM Series.

[33] P. Hakansson, D. Wang and S. Gong, "An Ultra-Wideband Six-port I/Q Demodulator Covering from 3.1 to 4.8 GHz," *ISAST Transactions on Electronics and Signal Processing*, no.1, vol. 2, pp. 16 – 20, 2008.

[34] Shaofang Gong, Magnus Karlsson, Adriana Serban, Joakim Östh, Owais, Jaap Haartsen and Peter Karlsson, "Radio Architecture for Parallel Processing of Extremely High Speed Data," *2009 IEEE*

International Conference on Ultra-Wideband, Sep. 2009, Vancouver, Canada. (*Paper VI*).

[35] International Technology Roadmap for Semiconductors (ITRS) website: www.itrs.net.

[36] M. Karlsson, and S. Gong, "A frequency-triplexed inverted-F antenna system for ultra-wide multi-band Systems 3.1-4.8 GHz," *ISAST Transactions on Electronics and Signal Processing*, no.1, vol. 1, pp. 95 – 100, 2007.

[37] M. Karlsson, and S. Gong," Circuit Dipole Antenna for Mode 1 UWB radio with Integrated Balun Utilizing a Flex-rigid Structure," *IEEE Transactions on Antennas and Propagation*, to be published.

[38] M. Karlsson, P. Håkansson and S. Gong," A frequency triplexer for ultra-wideband systems utilizing combined broadside- and edge-coupled filters," *IEEE Transactions on Advanced Packaging* vol. 31, no. 4, pp.794 – 802, Nov. 2008.

[39] A. Serban and S. Gong, "Low-Noise Amplifier Design at 5 GHz, in *Proc. The IMAPS Nordic Annual Conference*, 2005, Tønsberg, Norway, p. 227 – 229.

[40] A. Serban and S. Gong, "Ultra-wideband Low-Noise Amplifier Design for 3.1-4.8 GHz," in *Proc. GigaHertz 2005 Conference*, Uppsala, Sweden, pp. 291 - 294.

CHAPTER 3 WIDEBAND TRANSMITTERS AND RECEIVERS

Modern transceiver solutions are adapted to the severe constraints derived from the narrow bandwidth operation: narrowband amplification and filtering, bandwidth-efficient modulation. Moreover, they are thought such they can take advantage of the strengths of CMOS technology, circumventing its weaknesses. Today, the spectacular popularity of short-range, high data rate wireless transmission, has led to a new situation, the interest in wideband transmission. Covering a broad bandwidth is quite a challenging task that requires modifications at both circuit and system level. From transceiver operation confined within kHz-wide bands to hundreds of MHz operation, the design of UWB systems faces new issues: broadband LNAs, mixers and oscillators operating at higher frequency, the necessity of broadband matching and accurate component modeling over a wide bandwidth. On system-level, trying to simplify the generation and detection of signals while taking advantage of the existing and well-established narrowband transceiver solutions, the multiband orthogonal frequency-division multiplexing (OFDM) operation is considered. However, it remains still to cover 528-MHz bands. This chapter is aimed to give a better insight of the necessary trade-offs and limitations in transceiver architectures for UWB applications. Firstly, traditional receiver and transmitter architectures are briefly presented. Then, recently reported UWB receivers and transmitters are analyzed. The impact of the UWB system specification in terms of fractional bandwidth and power level on the RF front-end topologies and circuit solutions, challenges and trade-offs are finally concluded. This chapter reflects a part of the research which has been presented in *Paper II*, *Paper VI* and *Paper VII*.

3.1. Introduction to Wideband Transceiver Design

The basic function of a wireless transceiver is very simple: in the transmitter path, a high-frequency carrier is modulated by the "information signal", called *baseband* signal. The baseband signal can be an analog or digital waveform from a microphone or from a digital circuit [1]. In order to be transmitted by the antenna, the modulated carrier is amplified by a power amplifier (PA). In the receiver path, after being received by the antenna, the modulated *passband* signal is amplified by the low-noise amplifier, down-converted and finally demodulated. In this way, the original information that was sent from the transmitter is recovered.

In realistic environment, the received modulated signal is corrupted by noise and attenuated. Moreover, as shown in previous chapters, for UWB transmitter specifications the signal is very weak, while other strong unwanted signals might co-exist in the vicinity or even within the allocated spectrum. Furthermore, the communication medium can generate reflections from different obstacles, suppressing the desired signal by destructive interference. All these system specifications, operation condition, as well as the worst case scenarios make the design of any wireless transceiver and particularly of the UWB transceiver a difficult task.

The performance of a generic transceiver is usually quantified in terms of its range, i.e., the maximum distance across which it operates while providing satisfactory reception [2]. Complexity, power consumption and cost are primary criteria in selecting transceiver architectures. As new wireless communication standards continuously emerge enabling for higher and higher data rates, the importance of different criteria in choosing the transceiver architecture changes. The technology for RF transceiver for UWB wireless communications is dominated today by the integrated circuit (IC) technology, with GaAs and SiGe bipolar processes offering the best RF performance. In terms of system integration and integrated circuit (SoC) cost, the ideal solution is the CMOS technology, i.e., the RF transceiver as a SoC extensively using the digital power of processing signals.

As discussed in previous chapter, the CMOS implementations of RF circuits has a series of limits, some of them being now considered "traditional bottlenecks",

i.e., the integration of passive components. They seem “to ignore” the extraordinary progress of the CMOS technologies while being indispensable in almost every circuit in the transceiver chain.

New challenges generate new solutions. The UWB technology is one of the promising technologies for Gbit/s data transmission distinguished among other modern technologies by the huge available bandwidth. In the R&D media around the world and in this thesis, new and old approaches are investigated and adapted to the challenges aroused by the UWB transceiver specification. At a closer look, a majority of the reported UWB receiver and transmitter accommodate classical narrowband circuit topologies and receiver and transmitter architectures to wideband operations with inherent trade-offs.

3.2. Transceiver Principle

For a better insight of the implications resulting from UWB specifications, conventional transceiver architectures are shortly presented and then exemplified with recent IC implementation for UWB applications.

A Transmitter Topologies

The core function of a transmitter is to generate the modulated signal at the desired carrier frequency f_c. Generalized transmitter topologies can be derived from equations describing any modulated signal $s(t)$ [1]:

$$s(t) = A(t)\cos[\omega_c t + \varphi(t)] \tag{3.1a}$$

$$s(t) = s_I(t)\cos\omega_c(t) - s_Q(t)\sin\omega_c t \tag{3.1b}$$

where $A(t)$ and $\varphi(t)$ are the modulated amplitude and modulated phase, respectively and $\omega_c = 2\pi f_c$ is the angular frequency associated with the carrier frequency f_c. Equation (3.1b) illustrates the quadrature upconversion process: the in-phase and quadrature-phase baseband signals $s_I(t)$ and $s_Q(t)$ generated by the baseband circuits are up-converted by separately mixing them with two quadrature LO signals, a sine and a cosine. Given the high frequency of the carrier signals today, practical transmitters may perform the modulation at a lower intermediary frequency (IF) and then up-convert to the desired carrier frequency. Hence, there are basically two transmitter topologies: direct up-

conversion and dual up-conversion or heterodyne up-conversion as shown in Figure 3.1a and 3.1b, respectively [2].

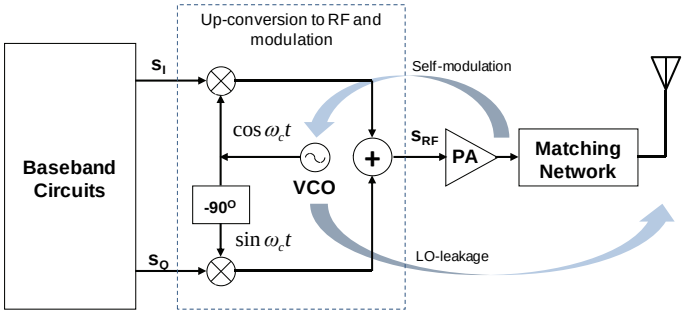

(a)

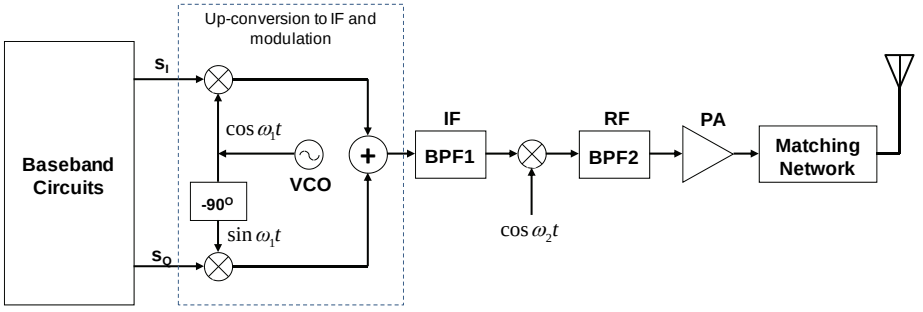

(b)

Figure 3.1. (a) Direct-conversion transmitter, (b) dual-conversion transmitter architecture.

Direct-conversion transmitters directly convert the baseband signals $s_I(t)$ and $s_Q(t)$ to the carrier frequency. As shown in Figure 3.1a, the local oscillator (LO) frequency is equal with the carrier frequency and the modulation and upconversion occur in the quadrature modulator simultaneously. In Figure 3.1b, the heterodyne transmitter performs the modulation firstly to an intermediary frequency (IF), ω_1. Then, by mixing and filtering, the modulated signal is translated to the carrier frequency equal with $\omega_1 + \omega_2$. In both cases, the modulated signal is then amplified by a power amplifier (PA). The matching network in Figure 3.1 has a double role: to provide maximum power transfer to

the wideband antenna and filter out-of-band components which usually occur due to the power amplifier non-linearity.

Transmitter performance can be characterized in terms of:

I/Q Mismatch As shown by (3.1a) and (3.1b) and illustrated in Figure 3.1, phase- and amplitude-modulated signals requires accurate quadrature LO signals. Errors in the nominal $\pi/2$-shifted LO phase, and mismatches between I- and Q-paths corrupt the up-converted signal constellation [2]. The main drawback of the direct-conversion transmitter is that modulation is performed at the carrier frequency, where perfect in- and quadrature-phase LO signals are difficult to achieve. In the dual-conversion transmitter, the quadrature modulation is performed at lower frequency (IF). This reduces the sensitivity of the modulated signal to quadrature errors (amplitude and phase errors).

LO leakage Leakage of the LO signal to the antenna appears due to poor isolations between the LO and RF ports of a mixer. As the LO frequency is equal with the carrier frequency, the LO leakage cannot be suppressed by means of a bandpass filter in a direct-conversion transmitter. The LO leakage increase the system power consumption, deform the modulated signal and can affect correct signal demodulation [3].

Self-modulation Known also as “injection locking” [2], self modulation appears when a large power modulated signal at the output of the PA is fed back to the VCO and corrupts the oscillator spectrum. The phenomenon of self-modulation is alleviated in a heterodyne transmitter as the carrier frequency at the output of the PA is different from the LO frequency (IF). However, in a direct-conversion transmitter topology for UWB applications, self-modulation might not be an issue as the transmitted power is very low.

Self-modulation and LO leakage are the two main drawbacks of any direct-conversion transmitter. Trying to preserve the signal quality, the quadrature dual-conversion transmitter requires an increased number of analog circuits, i.e., mixers, filters, resulting in increased power consumption. Moreover, to accommodate UWB standards, the demand for wider bandwidths complicates the design of all analog circuits in the transmitter chain [3].

B Receiver Topologies

The receiver front-end has to be able to process very small signals at very high frequency in a noisy environment and in the presence of other large, unwanted signals. Due to these operation conditions, receiver front-ends are much more complex than transmitter front-ends. They are dominated by analog circuits such as LNA, mixers and filters and have been implemented in a large variety of architectures: direct-conversion (homodyne), heterodyne, super-heterodyne, low-IF and wideband receivers are only a few of them. The principal receiver architectures reflect hardware solutions to different problems emerging from the down-conversion process of the modulated signals. In Figure 3.2a and 3.2b, the simplified direct-conversion (homodyne, zero-IF) and dual-conversion (heterodyne) receiver topologies are shown, respectively.

Direct-conversion (homodyne, zero-IF) receivers convert directly the RF signal to the baseband. As illustrated in Figure 3.2a, the signal received from the antenna is firstly filtered and amplified by the LNA. After amplification, the RF signal is down-converted to the baseband quadrature signals I and Q. For multi-carrier applications, the LO signal is tuned to down-convert the selected channel. Low-pass filters attenuate the adjacent channels and following variable gain amplifiers (VGA) adjust the I- and Q-signal level before the analog-to-digital (A/D) conversion.

The dual-conversion (heterodyne) receiver architecture is one of the most popular architectures for today's receiver in wireless communication systems. The down-conversion to the baseband of the received RF signal can be performed in different modes. In Figure 3.2a, the received signal is passed firstly through a band-pass filter (BPF1) which suppresses the out-of-band interferers. The LNA amplifies the weak signal which is further filtered by a second band-pass filter, BPF2. Its role is mainly to reject the image frequency located at a distance of $2f_{IF}$ from the desired channel (carrier) frequency [2]. In the following first mixer (Mixer 1), the RF signal is mixed with the local oscillator (LO1) signal to get a lower intermediary frequency (IF). For multi-carrier receivers, the LO1 can be tuned to select the desired channel. The second down conversion is a quadrature down-conversion from IF to baseband. After demodulation, the I and Q baseband signals are filtered with a band-pass filter BPF3 and amplified by variable-gain amplifiers (VGA) to compensate for the losses in the band-pass

filters and to get an optimal amplitude to the following analog-to-digital convertors (ADC).

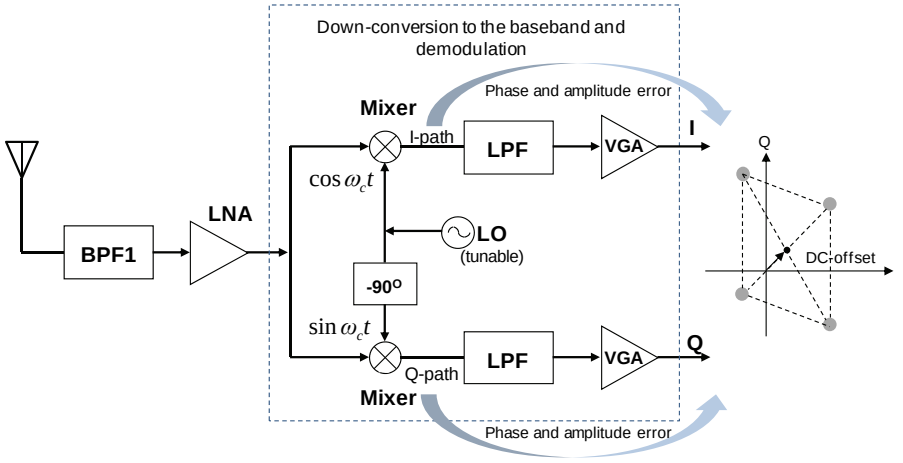

(a)

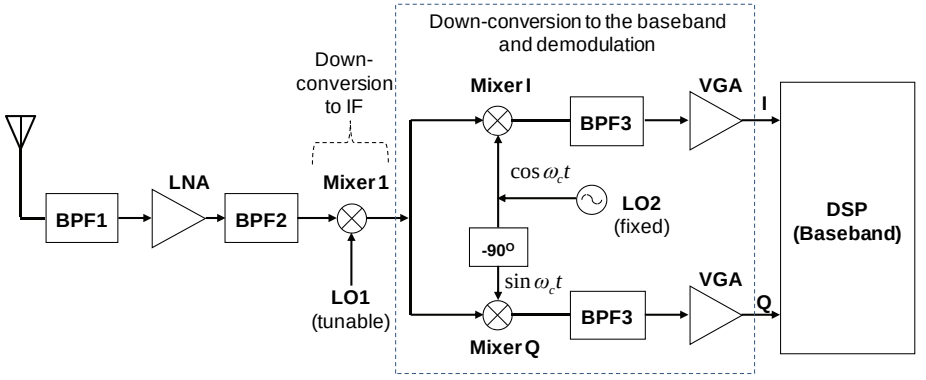

Figure 3.2. Receiver topologies: (a) Direct-conversion with effect of I/Q mismatch and LO leakage, and (b) dual-conversion (heterodyne) topology.

The main architecture-related problems in receivers are:

I/Q Mismatch As in the case of the transmitter, phase- and amplitude-imbalance of the quadrature LO signals, and mismatches between I- and Q-paths corrupt the down-converted signal constellation [2]. In the direct-conversion receiver, they cause *static* dc-offset [5]. Direct down-conversion from GHz-frequencies requiring accurate *quadrature* LO generation at carrier frequencies can explain partially amplitude and phase mismatches. Layout- and component parameter tolerance generate also mismatches and contribute to static dc-offset. The static dc-offset can be improved by different DSP-based compensation methods. In the dual-conversion transmitter, the quadrature modulation is performed at lower frequency (IF). This reduces the sensitivity of the modulated signal to quadrature errors (amplitude and phase errors).

LO leakage The LO leakage generates *time-varying* dc-offsets. The receiver LO leakage can be explained by the insufficient isolation between the LO and RF ports in mixers and LNA due to parasitic, feedthrough paths as shown in Figure 3.2. The LO signal can be fed back to the input of the LNA and amplified to the input of the mixer. By mixing with the original LO signal (*self-mixing*), an unwanted time-varying dc component at the output of the mixer is generated. In a direct-conversion receiver, the dc-offset is superimposed on the baseband signals corrupting them. In *multi-band* transceiver with multiple carrier spread over a large frequency spectrum, the dc-offset can vary significantly when the LO frequency changes. Moreover, dc-offsets are also caused by the presence of the transmitter LO-leakage.

Generally, transmitter and receiver LO leakage in direct-conversion transceivers increase the system power consumption, deform the modulated signal and can affect correct signal demodulation [3]-[4].

Receiver performance parameters are:

Noise Figure Noise can generally be defined as any unwanted signal in a transmission system [2]. Noise in a transmission system can be caused by different sources. In the receiver part, the total noise figure is dominated by the noise figure of the first active stage, i.e., the LNA, limiting the sensitivity of the receiver. The main types of noise mechanisms are thermal noise, shot noise and

flicker noise. The receiver noise figure is the noise metric showing how much the signal degrades when passing through a device and is defined as:

$$NF = \frac{SNR_{in}}{SNR_{out}} = \frac{S_{in}/N_{in}}{S_{out}/N_{out}} \tag{3.2}$$

where SNR_{in} and SNR_{out} are the signal-to-noise ratios measured at the input and output, respectively. S_{in} is the input signal and S_{out} is the output signal. N_{in} is the noise at the input and N_{out} is the noise at the output.

As shown in Chapter 2, Friis equation shows that the overall front-end noise figure NF_{tot} is dominated by the noise figure of the first stage, NF_1, i.e., the noise figure of the LNA. The gain of the LNA, G_1, reduces noise contribution of the subsequent circuits in the front-end.

Sensitivity is one of the most important parameters which characterize the communication system performance. It is defined as the minimum input signal level that can be detected having a specified output signal-to-noise ratio, SNR_{out}:

$$Sensitivity = P_{in,min} = -174dBm/Hz + NF + 10logBW + SNR_{out} \tag{3.3}$$

where -174 dBm represents the noise power that the source resistance delivers to the receiver, assuming conjugate matching at the receiver input. From (3.3), the minimum input signal depends on the bandwidth (BW) of the system, the noise figure (NF) of the receiver and the output signal-to-noise ratio (SNR_{out}) [2]: Communication reliability and radio range depend directly on the smallest signal that a receiver can process. According to (3.3), noise limits the smallest signal that a receiver can process, and thus the receiver sensitivity.

Selectivity in multiband radio systems shows the ability of a radio receiver to select a particular channel (sub-band) while rejecting the other frequencies. Other unwanted frequencies can be modulated signals in adjacent channels, or other interferers from co-existing standards. The selectivity is determined by the characteristic of RF, IF and baseband filters. The frequency plan adopted to convert the RF signal to the baseband and different receiver architectures result in different filter requirements within the receiver chain. In wideband receivers, the LNA is usually a broadband circuit and in this case the selectivity is mainly determined by a channel select filter placed after the mixer.

3.3. Reported UWB Transceiver Architectures

Trying to categorize the existing UWB receivers, three approaches to the RF receiver front-end can be identified: *multipath* narrowband homodyne, wideband homodyne and wideband heterodyne. All these UWB transceiver solutions exploits the MBOA (MB-OFDM) partition of the UWB spectrum into 528-MHz bands [5].

Taking a closer look to the multipath homodyne receiver in Figure 3.3a, separate signal paths are used for each band of Mode 1 MB-OFDM [6]. In this way, narrowband approaches can be applied for optimizing each path on the cost of increased power consumption and consumed area. The UWB LNA is implemented using broadband common-gate (CG) stage which provides an input resistance of 50 Ω. It has three resonant loads corresponding to the three bands and totally four on-chip inductors, increasing the area, noise figure and design complexity.

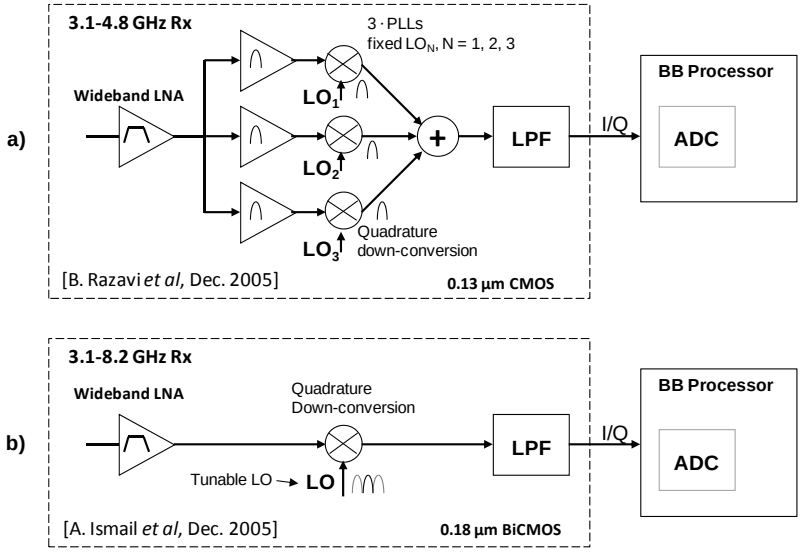

Figure 3.3. UWB receiver architectures. (a) Multipath direct-conversion [6], (b) wideband direct conversion [7].

Similar LNA topology is discussed in Appendix A2. The LNA is driving three selectable quadrature mixers. Moreover, the complexity of the multiband receiver design in Figure 3.3a and its power consumption are increased due to the use of three on-chip phase-locked loops (PLLs). In this case, exploiting the wide bandwidth through a multiband solution, the information is supposed to be interleaved across all three bands. As the band switching must occur in less than 9.47 ns [6], which is a very short settling time for any PLL, three-PLLs are integrated, one for each band's LO frequency. In addition, the PLLs must generate accurate in-phase and quadrature-phase LO signals.

In the second approach of MB-OFDM receiver shown in Figure 3.3b [7], the wideband LNA is an inductively degenerated common-emitter (CE) amplifier stage with an input matching network, as presented in Appendix A1. After amplification, the signal is direct converted to the baseband. The local oscillator signals are generated by a direct digital frequency synthesizer (DDS). Frequency tuning is done by switching among the different frequencies. The wanted band at 0 Hz is low-pass filtered to attenuate the adjacent channels.

In the third UWB transceiver shown in Figure 3.4, one of the few dual-conversion topology approaches [8] for MB-OFDM is presented. After amplification, the 3.1-8.0 GHz signal is firstly down-converted to IF1 at 2.9 GHz and then to IF2 at dc. The receiver and transmitter share the first RF mixer reducing the capacitive loading of the frequency synthesizer. The second down-conversion employs quadrature (IQ) mixer at lower frequency. The baseband output signal with 264 MHz bandwidth is processed by an on-chip 6-bit ADC with a sampling frequency of 528 MHz to generate the final binary output bits. On the transmitter side, a 6-bit DAC generate I- and Q signals to be up-converted. Due to the UWB low transmit power specifications, in TX-Mode no power amplifier is used. Instead, a simple buffer is added for output matching and desired power levels.

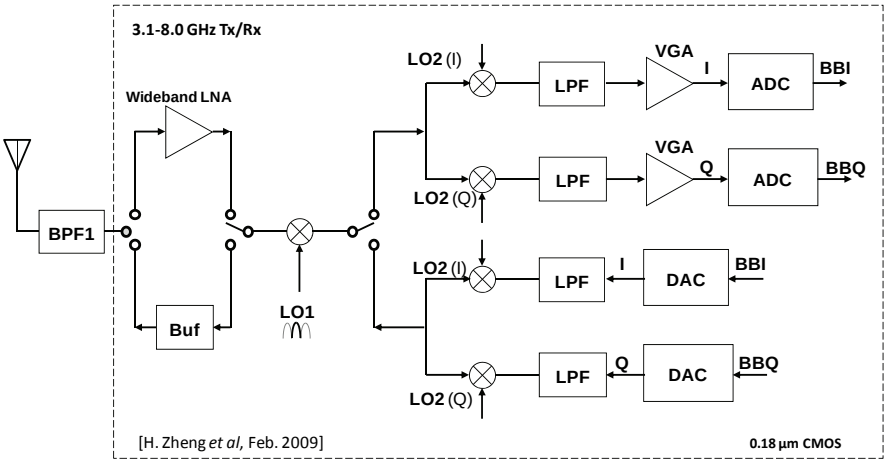

Figure 3.4. UWB transceiver heterodyne architecture [8].

3.4. Six-Port Transmitters and Receivers

As shown in the previous Section, when discussing wireless transceiver solutions for 3.1 - 10.6 GHz UWB it is almost synonym with referring to receivers and transmitters integrated on a chip using SiGe bipolar or CMOS processes. We have also seen that despite progresses in the RF CMOS IC field, CMOS is not yet the perfect solutions for any RF circuit and particularly not for UWB circuits.

In order to overcome some of the problems of the UWB radio solutions at circuit and system level in CMOS and BiCMOS technologies, unconventional radio solutions for 3.1-4.8 GHz UWB applications based on the six-port network were reported in 2006 [9]-[10]. However, the idea to use a six-port network in a receiver configuration was introduced and successfully proofed already in 1994 [11]-[12]. Since then, the unconventional receivers with six-port network have been intensively studied mainly for Ka-band (26-40 GHz), V-band (50-75 GHz) and for the new millimeter-wave (mm) band at 60 GHz (57-64 GHz) Wireless Personal Area Networks (WPAN) applications [7]-[9]. Promising very high data rates, these six-port radio and radar front-ends are implemented as Microwave Hybrid Monolithic Integrated Circuit (MHMIC) or Microwave Monolithic Integrated Circuit (MMIC) [10].

3.4.1. The Six-Port Correlator

The six-port correlator (also known as six-port junction, six-port network) is a passive microwave circuit usually implemented in MHMIC and MMIC technologies. Various configurations of the six-port circuit are based on different combinations of power dividers and four-port hybrids interconnected by transmission lines [17]. They can be divided into three types of six-port configurations [18]:

Six-port circuit of type A shown in Figure 3.5a is a typical, widely used six-port configuration with one Wilkinson power divider and three quadrature (90°) branch-line couplers [19].

Six-port circuit of type B consists of two power dividers, 90° branch-line couplers and two 45° phase shifters, as shown in Figure 4.1b [20].

Six-port circuit of type C in Figure 4.1c consists of four 90° branch-line couplers and one 90° phase shifter [21].

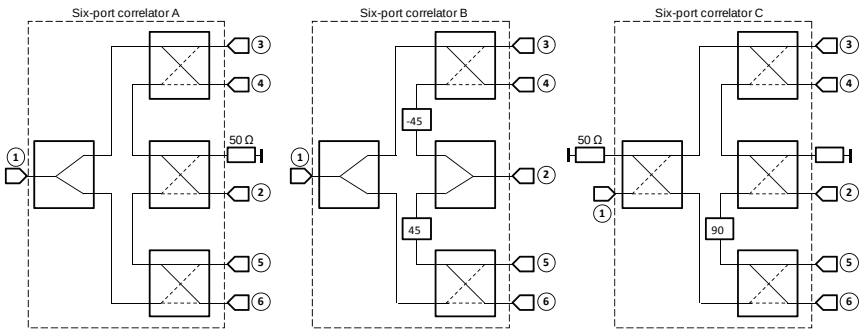

Figure 3.5. Six-port circuit configurations, [18].

For a given configuration, the six-port network can be described by means of the scattering ([S]-) parameters which relate the reflected and incident normalized power waves, a_i and b_i, respectively

$$\begin{bmatrix} b_1 \\ \vdots \\ b_6 \end{bmatrix} = \begin{bmatrix} S_{11} & \dots & S_{16} \\ \vdots & \ddots & \vdots \\ S_{16} & \dots & S_{66} \end{bmatrix} \begin{bmatrix} a_1 \\ \vdots \\ a_6 \end{bmatrix} \tag{3.4}$$

The linear relationship between normalized power parameters and incident and reflected voltage waves at port i, i = 1 to 6, is given by [22]

$$v_i^+ = \sqrt{Z_0}a_i \tag{3.5}$$

$$v_i^- = \sqrt{Z_0}b_i \tag{3.6}$$

The design requirements and also the non-idealities of the six-port network can be understood by the analysis of the six-port scattering (S-) matrix. For the six-port network of type A shown in Figure 3.6, the S-matrix can be derived using the S-parameters of ideal Wilkinson power divider and 90° branch-line coupler. Firstly, it is assumed that all ports are matched and the delay of the interconnections is ignored. Secondly, it is also assumed that one quarter-wave (λ/4) transmission line within the Wilkinson power divider and 90° branch-line couplers ideally contribute with a phase shift of -90°, in phasor form corresponding to e^{-j90^0} [17]. Following the analytical methodology in [17], the [S]-matrix of the ideal six-port network of type A is given by

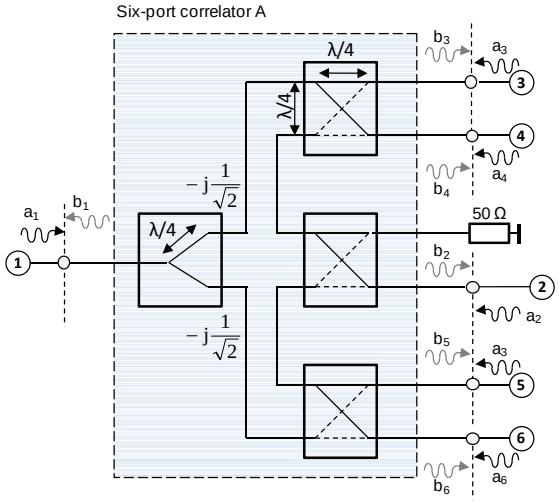

Figure 3.6 Ideal six-port network type A with incident and reflected normalized power waves, a_i and b_i at port i, i = 1 to 6.

$$[S]=\frac{1}{2}\begin{bmatrix} 0 & 0 & e^{-j180} & e^{-j270} & e^{-j270} & e^{-j180} \\ 0 & 0 & e^{-j0} & e^{-j270} & e^{-j180} & e^{-j270} \\ e^{-j180} & e^{-j0} & 0 & 0 & 0 & 0 \\ e^{-j270} & e^{-j270} & 0 & 0 & 0 & 0 \\ e^{-j270} & e^{-j180} & 0 & 0 & 0 & 0 \\ e^{-j180} & e^{-j270} & 0 & 0 & 0 & 0 \end{bmatrix} = \frac{1}{2}\begin{bmatrix} 0 & 0 & -1 & +j & +j & -1 \\ 0 & 0 & 1 & +j & -1 & +j \\ -1 & 1 & 0 & 0 & 0 & 0 \\ +j & +j & 0 & 0 & 0 & 0 \\ +j & -1 & 0 & 0 & 0 & 0 \\ -1 & +j & 0 & 0 & 0 & 0 \end{bmatrix} \tag{3.7}$$

The general relationships between reflected and incident normalized power waves at each port of the ideal six-port network become

$$b_1 = \frac{1}{2}(-a_3 + ja_4 + ja_5 - a_6) \tag{3.8a}$$

$$b_2 = \frac{1}{2}(a_3 + ja_4 - a_5 + ja_6) \tag{3.8b}$$

$$b_3 = \frac{1}{2}(-a_1 + a_2) \tag{3.8c}$$

$$b_4 = \frac{1}{2}(ja_1 + ja_2) \tag{3.8d}$$

$$b_5 = \frac{1}{2}(ja_1 - a_2) \tag{3.8e}$$

$$b_6 = \frac{1}{2}(-a_1 + ja_2) \tag{3.8f}$$

With regard to the S-parameters in (3.7), six-port general design goals can be derived:

Low value S_{11} and S_{22}: it can be achieved by accurate design of the six-port network for 50 Ω input impedance at the central frequency over the desired frequency band.

Good isolation between ports 1 and 2: a special attention should be paid to the optimization of the 90° branch-line couplers design. Good matching at all ports.

Low value S_{33}, S_{44}, S_{55}, S_{66}: it can be achieved by good impedance matching at ports 3 to 6 and optimization of the 90° branch-line coupler design over the desired band.

*Low value S_{34}, S_{56}, etc.: by o*ptimization of the 90° branch-line coupler design.

Phase shift n x 90° rule, n = integer: the phase shift relationship between different ports should be kept as close as possible to the theoretical values shown in (3.7). Layout techniques such as common-centroid symmetry and layout miniaturization are required.

Amplitude balance: the signal attenuation should be maintained as closed as possible to -6 dB from port to port within the desired paths through appropriate layout techniques.

Adding other passive or active devices to the six-port networks in Figure 3.6, microwave signal processing can be performed. Port 1 and port 2 are usually dedicated to the LO (reference signal) and RF modulated signals, respectively. Port 3, 4, 5 and 6 are either connected to different impedance terminations via RF switches (in six-port modulator applications) or to power detectors (in six-port demodulator applications). Unused ports are terminated with the system characteristic impedance, usually 50 Ω. On one hand, once the equations (3.8) are determined for the desired six-port topology, the entire mathematical model of the specific six-port applications (modulator, demodulator, radar) can be deduced. On the other hand, this theoretical model will explain the operation principle and will support the comparison between conventional and six-port radio architectures.

3.4.2. The Six-Port Modulator

Since 1990s the six-port network has been primarily used in direct-conversion receiver schemes. In 2005 the first direct-carrier QPSK six-port modulator was successfully introduced as an alternative to conventional quadrature modulators used in dual-conversion transmitters [23]. The six-port modulator in [23]-[24] is shown Figure 3.7. It included the six-port correlator (type A), four RF switches, and four terminations of ideal zero (SHORT) and ∞ (OPEN) values. At port 1 the local oscillator (LO) signal $s_{LO}(t) = A_{LO}\cos \omega_{LO}t$ is fed, where A_{LO} and ω_{LO} are the amplitude and angular frequency, respectively. The output RF signal $s_{RF}(t)$ results at port 2. At port 3 to 6, the RF switches controlled by the baseband data generate reflection coefficients of two values, Γ_i = -1 and Γ_i = +1, corresponding to SHORT and OPEN impedance termination conditions, respectively.

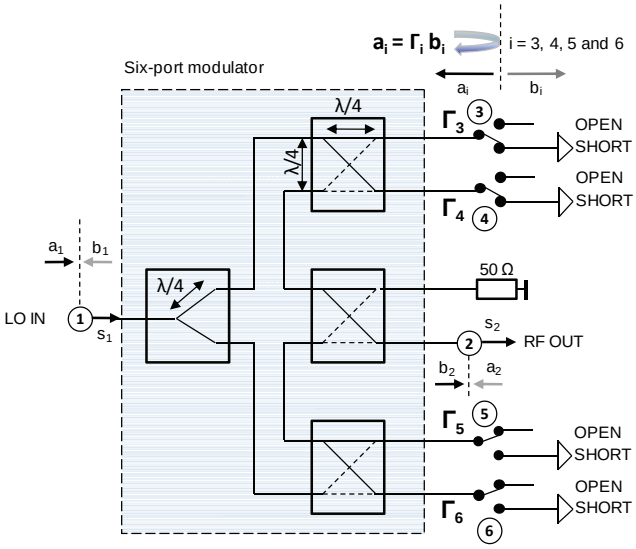

Figure 3.7. Six-port modulator with SHORT and OPEN terminations.

Using the input and output signal assignments illustrated in Figure 3.7, and assuming perfect matching at port 1 and 2, the normalized power waves can be particularized as

$$a_1 = \mathrm{s_{LO}}(t)/\sqrt{Z_0} = A_{LO}\cos\omega_{LO}t/\sqrt{Z_0} \tag{3.9}$$

$$b_1 = 0 \tag{3.10a}$$

$$a_2 = 0 \tag{3.10b}$$

$$a_i = \Gamma_i b_i, \quad \mathrm{i} = 3, 4, 5 \text{ and } 6 \tag{3.11}$$

Then, from (3.8b) and (3.8c)-(3.8f), and (3.11), the output signal of the six-port circuit in Figure 3.7 can be calculated

$$b_2 = -\frac{1}{4}\, a_1[\Gamma_3 + \Gamma_4 + j(\Gamma_5 + \Gamma_6)] \tag{3.12}$$

Or, using (3.5) and (3.6), the output RF signal of the six-port modulator can be expressed as a function of complex voltage signals

$$s_{\mathrm{RF}}(\mathrm{t}) = -\frac{1}{4} s_{\mathrm{LO}}(\mathrm{t})[\Gamma_3 + \Gamma_4 + j(\Gamma_5 + \Gamma_6)] \tag{3.13a}$$

Moreover, assuming the particular case $\Gamma_3 = \Gamma_4$ and $\Gamma_5 = \Gamma_6$, $s_{\mathrm{RF}}(\mathrm{t})$ becomes

$$s_{\mathrm{RF}}(\mathrm{t}) = -\frac{1}{2} s_{\mathrm{LO}}(\mathrm{t})\left[\Gamma_I + j\Gamma_Q\right] \tag{3.13b}$$

In time domain, the RF signal can also be written as

$$s_{\mathrm{RF}}(\mathrm{t}) = -\frac{\mathrm{A_{LO}}}{2}\sqrt{\Gamma_{\mathrm{I}}^2(\mathrm{t}) + \Gamma_{\mathrm{Q}}^2(\mathrm{t})}\cos\left(\omega_{\mathrm{LO}} t + \tan^{-1}\left(\frac{\Gamma_{\mathrm{Q}}(\mathrm{t})}{\Gamma_{\mathrm{I}}(\mathrm{t})}\right)\right) \tag{3.13c}$$

Firstly, equations (3.13a)–(3.13c) depicts that the six-port circuit in Figure 3.7 uses both in-phase (Γ_{I}) and quadrature (Γ_{Q}) components to generate the output signal $s_{\mathrm{RF}}(\mathrm{t})$. Secondly, the mathematical model based on the six-port network S-parameters shows that the amplitude and phase of the output RF signal depend on the reflection coefficients Γ_{i}, (i = 3, 4, 5, 6). In fact, (3.13c) can be identified as a quadrature modulated signal as classically expressed in radio-system terminology [1].

$$s(t) = A(t)\cos[\omega_c t + \varphi(t)] \tag{3.14a}$$

where $A(\mathrm{t})$ and $\varphi(\mathrm{t})$ are the modulated amplitude and modulated phase, respectively and $\omega_{\mathrm{c}} = 2\pi f_{\mathrm{c}}$ is the angular frequency associated with the carrier frequency f_{c}. Other useful equations can be derived from (3.14a)

$$s(t) = s_I(t)\cos\omega_c\,(t) - s_Q(t)\sin\omega_c\, t \tag{3.14b}$$

$$s_I(t) = A(t)\cos\varphi\,(t) \tag{3.15a}$$

$$s_Q(t) = A(t)\sin\varphi\,(t) \tag{3.15b}$$

$$A(\mathrm{t}) = \sqrt{s_{\mathrm{I}}^2(\mathrm{t}) + s_{\mathrm{Q}}^2(\mathrm{t})} \tag{3.16}$$

$$\varphi(\mathrm{t}) = \tan^{-1}\left(\frac{\mathrm{s_Q(t)}}{\mathrm{s_I(t)}}\right) \tag{3.17}$$

where $s_{\mathrm{I}}(\mathrm{t})$ is the in-phase modulation data, $s_{\mathrm{Q}}(\mathrm{t})$ is the quadrature modulation data. Finally, using the concept of complex envelope $g(\mathrm{t})$ [1] expressed both in Cartesian and in polar coordinates by

$$g(t) = s_I(t) + js_Q(t) = |g(t)|e^{j\varphi(t)} \tag{3.18}$$

the quadrature modulated signal can be written

$$s(t) = \mathcal{R}e\{g(t)e^{j\omega_c t}\} \tag{3.19}$$

where g(t) is the complex envelope of s(t), Re{•} denotes the real part of {•}.

An interpretation of (3.19) is that the spectrum of the baseband signal g(t) is translated up to the carrier frequency. The relationship between A(t), φ(t) and x_I(t), x_Q(t) for QPSK and 16-QAM signals are illustrated also in Figure 3.8.

In conclusion, the output signal of the six-port circuit in Figure 3.7 expressed by (3.13)-(3.14) demonstrate that direct-carrier multi-level quadrature amplitude modulation (M-QAM) can be theoretically obtained with the six-port modulator technique. It also results that the six-port modulator in Figure 3.7 with two states (SHORT and OPEN) for Γ_I and Γ_Q generates QPSK modulated signals. Other modulations, suitable for high data rate transmission, such as 16-QAM or 64-QAM can be generated if more than two states for the reflections coefficients can be implemented and controlled by the I- and Q-baseband data.

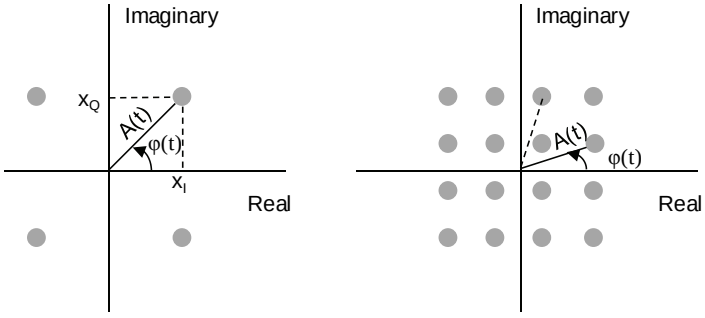

(a) (b)

Figure 3.8. QPSK and 16-QAM constellations.

3.4.3. The Six-Port Demodulator

In the six-port receiver shown in Figure 3.9, a local oscillator (LO) signal of frequency ω_{LO} is applied to port 1 of the six-port network. The received RF modulated signal enters port 2 with the carrier frequency ω_c. Matched pairs of zero-biased Schottky diode power detectors provide mixing function by squaring the signals at port 3, 4, 5 and 6. After the diodes, high frequencies terms are low-pass filtered and the I- and Q-signals are obtained by means of two differential amplifiers [13].

Using the same methodology based on the S-parameters given by (3.7) of the six-port network, the transfer functions of the six-port receiver can be determined. Firstly, the input LO signal and RF modulated signal in time domain are

$$s_1 = s_{LO}(t) = A_{LO} \cos \omega_{LO} t \tag{3.20a}$$

$$s_2 = s_{RF}(t) = A_{RF}(t) \cos[\omega_c t + \varphi_{RF}(t)] \tag{3.20b}$$

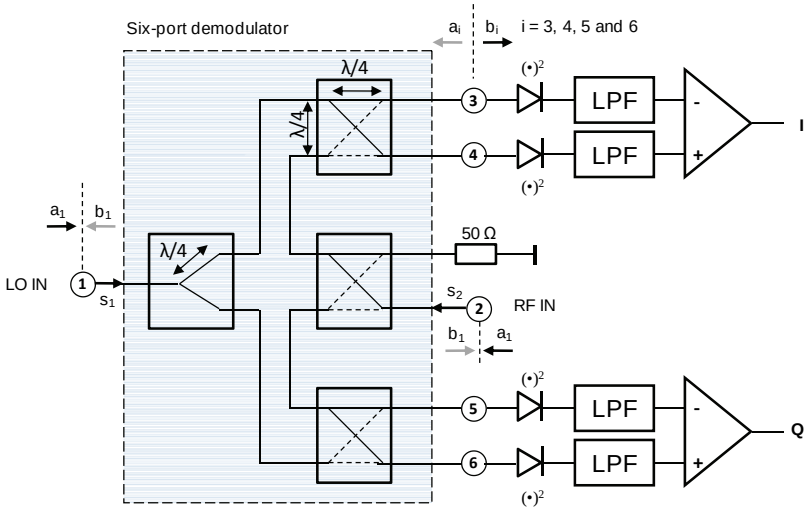

Figure 3.9. Six-port demodulator [13].

Secondly, assuming perfect matching at LO and RF ports (b_1 and b_2 = 0) and at the output ports 3, 4 and 5, 6 of the six-port, and using (3.8c)-(3.8d) expressed directly as voltage waves ($s_i(t)$ instead of a_i, b_i), the output signals at ports 3, 4, 5

and 6 can be written as a linear combination of the incident LO and RF signals, s_{LO} and s_{RF}

$$s_3(t) = \frac{1}{2}(-s_{LO} + s_{RF}) \tag{3.21a}$$

$$s_4(t) = \frac{1}{2}(\,\mathrm{j}s_{LO} + \mathrm{j}s_{RF}) \tag{3.21b}$$

$$s_5(t) = \frac{1}{2}(\mathrm{j}s_{LO} - s_{RF}) \tag{3.21c}$$

$$s_6(t) = \frac{1}{2}(-s_{LO} + \mathrm{j}s_{RF}) \tag{3.21d}$$

After passing through the six-port network, the signals at ports 3 to 6 in (3.21) are nonlinearly processed by zero-bias diodes. Neglecting the dc component in the Taylor series describing the nonlinear operation of the diode [13], squaring operation on (3.21) and following low-pass filtering (LP) of the high-frequency components at $2f_{LO}$, $2f_{RF}$ and $f_{LO} + f_{RF}$ yields:

$$\mathrm{LP}[s_3^2(t)] = \frac{A_{LO}^2}{8} + \frac{A_{RF}^2(t)}{8} - \frac{A_{LO}A_{RF}(t)}{4}\cos\Delta\Omega \tag{3.22a}$$

$$\mathrm{LP}[s_4^2(t)] = \frac{A_{LO}^2}{8} + \frac{A_{RF}^2(t)}{8} + \frac{A_{LO}A_{RF}(t)}{4}\cos\Delta\Omega \tag{3.22b}$$

$$\mathrm{LP}[s_5^2(t)] = \frac{A_{LO}^2}{8} + \frac{A_{RF}^2(t)}{8} - \frac{A_{LO}A_{RF}(t)}{4}\sin\Delta\Omega \tag{3.22c}$$

$$\mathrm{LP}[s_6^2(t)] = \frac{A_{LO}^2}{8} + \frac{A_{RF}^2(t)}{8} + \frac{A_{LO}A_{RF}(t)}{4}\sin\Delta\Omega \tag{3.22d}$$

where following abbreviation is used:

$$\Delta\Omega = \omega_c t + \varphi_{RF}(t) - \omega_{LO} t \tag{3.23}$$

And the modulated amplitude of the RF signal is

$$A_{RF}^2(t) = s_I^2(t) + s_Q^2 \tag{3.24}$$

The desired *I* and *Q* baseband signal regeneration relies on (a) perfectly cancellation of the first two terms in (3.22) and (b) on regeneration of the carrier, i.e., $\omega_{LO} = \omega_c$. Cancellation of the first two terms and therefore, theoretically dc-

offset cancellation is achieved by using two differential amplifiers. Assuming $\omega_{\mathrm{LO}} = \omega_{\mathrm{c.}}$

$$s_I(t) = s_{4-3}(t) \cong A_{LO}A_{RF}(t)\cos[\varphi_{RF}(t)] \tag{3.25a}$$

$$s_Q(t) = s_{6-5}(t) \cong A_{LO}A_{RF}(t)\sin[\varphi_{RF}(t)] \tag{3.25a}$$

Hence, using the six-port network with the additional components shown in Figure 4.5, a frequency down-conversion and demodulation has taken place. The baseband signal can finally be expressed as

$$s_{\mathrm{BB}}(t) = \left(s_{\mathrm{I}} + \mathrm{j}s_{\mathrm{Q}}\right) \tag{3.26}$$

3.5. Wideband Transceiver Design– Summary

The successful design of radio transceivers is dependent on the possibility of integration of the circuits into the same substrate using a low-cost process. The demand for wide bandwidths supported by emerging UWB standards further complicates the use of conventional RF architectures in advanced CMOS processes, while increasing the complexity of the digital part.

A majority of the reported conventional UWB transceivers accommodate well-established narrowband transceiver solution and circuit solutions to wideband operation. In MB-OFDM UWB transceiver implementations, multiband operation increases the parallelism in RF analog signal processing. Consequently, the complexity of the transceiver design is increased. Present conventional transceiver architectures for UWB applications are RF analog-intensive and therefore, not suited to integration in submicrometer CMOS processes.

With focus on the defining attribute of a UWB technology, some challenges posed by the UWB receiver and transmitter design for high data rates are concluded:

Wideband circuits and wideband input impedance matching are required. The LNA at the receiver front-end should provide low noise figure and high gain at low current consumption over a large bandwidth: from 2.5 GHz for the European standard to 7.5 GHz for the U.S. standard, or, at least 528 MHz for MB-OFDM UWB devices. Drawbacks of integrating UWB LNA in CMOS

processes were presented in Chapter 2 and detailed in Appendix A.1. Moreover, they can be extrapolated on other RF circuits in the transceivers.

Quadrature modulation/demodulation over a wideband is demanded. Consequently, (a) accurate quadrature LO phases (cosine and sinus) must be generated at different high carrier- or IF-frequency. This issue is in fact embedded within the general problem of LO-signals generation and carrier recovery for UWB systems which is already a difficult task no matter if it is solved by analog synthesis technique based on PLLs or digital synthesis technique based on all-digital PLLs [6]-[8]. Moreover, (b) process as well as passive and active component tolerances make presented conventional transceiver topologies integrated in CMOS processes prone to gain and phase imbalances in the I- and Q-paths. Typically required complex compensation techniques in the digital domain make the overall design power-inefficient. Finally, (c) quadrature direct-or dual-conversion of frequency require an increased number of wideband mixers. To integrate the two mixers of a quadrature scheme in modern CMOS technologies with reduced available supply voltage is an increasingly challenging for RF designers.

Multi-level modulation is required even for UWB specifications in order to achieve multi-gigabit data rates, as shown in *Paper VI* [25]. This has impact on the system architecture and on several circuits

Linearity constraints are posed also by the multiband solution. Poor linearity can contribute to second-order distortion. Harmonic second-order distortion in channel 1 falls into channel 5 as it can be seen in Figure 1.3.

New linearity constraints that do not exist in narrowband systems are a challenging aspect in UWB design. Due to its large transmission band, UWB systems must be able to co-exist with other UWB devices and other narrowband systems. The co-existence between UWB and narrow-band wireless communication systems results at the circuit level in the need of enhanced linearity receiver specification [6].

Based on the previous analysis of the six-port transmitter and receiver operation, and comparing six-port transceiver with traditional wideband transceiver solutions, a series of advantages and differences can be concluded:

No accurate quadrature LO phases (cosine and sinus) must be generated at different high carrier- or IF-frequency when six-port modulator and demodulator are used, as illustrated in Figure 3.7 and Figure 3.9 respectively. As shown in Section 3.2, generation of accurate quadrature-LO signals is a major problem in conventional transmitter and receiver architectures. Moreover, the carrier-frequency generation block is usually a voltage-controlled oscillator (VCO) within frequency synthesizer feedback loop to compensate for frequency drift of the VCO with time and temperature. The necessity of quadrature signals contribute to the complexity of the frequency synthesizer and the power consumption is consequently increased.

Low-power consumption by passive, additive mixing instead of active multiplicative mixing is performed with six-port modulator and six-port demodulator topologies. The mathematical models in Section 3.6 and 3.7 demonstrate that complex signals with their desired phase relationship and amplitude balance can be obtained mainly by accurate design of the six-port network. As the six-port correlator is a microwave component implemented with distributed transmission lines, good control of its S-parameters can be obtained by using well-established design methodologies and advanced simulation tools. As shown in *Paper I*, manufacturing process tolerances have little influence on microstrip line properties and thus also on circuits implemented with distributed components of microstrips. In comparison, active multiplicative mixing relies on usually narrow band, power hungry stacked transistors in classical Gilbert cell configuration. Component parasitics, tolerances of active and passive components and poor layout can supplementary influence the quality of up- and down-converted signals in conventional transceiver topologies.

Reduced LO power is required for frequency down-conversion when the non-linear mechanism in zero-biased diodes is used [25].

Wideband processing of RF signals is possible due to passive up and down frequency conversion. As shown in *Paper II, VI* and *VII*, the six-port correlator itself can be designed for wideband operation and, in six-port transceivers the data rate limits are generally set by circuits preceding or following the six-port modulator and demodulator[26]-[28].

The dc-offset is theoretically eliminated and in practice minimized in six-port direct conversion receivers by the differential technique applied on the four

output signals of the six-port demodulator. In comparison, in classical direct-conversion receiver architecture the dc-offset cancellation is realized by complex, power-consuming DSP techniques. Moreover, using differential amplifiers, the amplitude of the LO signals does not need to have a certain value.

Low-cost modulator-antenna and antenna-LNA-demodulator integration on the same substrate is facilitated when printed circuit board processes can be used in conjunction with six-port technology, as discussed in *Paper III* and *V*.

3.6. References

[1] L. W. Couch, *Digital and Analog Communication Systems*, Prentice-Hall, 2001, Ch. 5.

[2] B. Razavi, *RF Microelectronics*, Prentice Hall, 1998.

[3] Z. Zisan, K. Mertens, M. Tiebout, S. Ek, S. Marsili, D. Matveev C. Sandner, "A 6–9GHz WiMedia UWB RF transmitter in 90 nm CMOS," Proceedings of the IEEE *Radio Frequency Integrated Circuits Symposium, 2008*, RFIC, 2008, pp. 39 – 42.

[4] M. Pui-In, U. Seng-Pan, R. P. Martins, "Transceiver Architecture Selection," *IEEE Circuits and Systems Magazine*, vol. 7, issue 2, 2007, pp. 6 – 25.

[5] *Multi-Band OFDM Physical Layer Proposal, IEEE 802.15-03/268r5*, Nov. 2003.

[6] B. Razavi, T. Aytur, C. Lam, F. R. Yang, K. Y. Li, R. H. Yan, H. C. Hang, C. C. Hsu, C. C. Lee, "A UWB CMOS Transceiver," *IEEE Journal of Solid-State Circuits*, vol. 40, no. 12, pp. 2555 - 2562, Dec. 2005.

[7] A. Ismail, and A. A. Abidi, "Synthesizer in 0.18-μm SiGe BiCMOS for Mode-2 MB-OFDM UWB Communication," *IEEE Journal of Solid-State Circuits*, vol. 40, no. 12, pp. 2573 - 2582, Dec. 2005.

[8] H. Zheng, S. Lou, D. Lu, C. Shen, T. Chan, and H. C. Luong "A 3.1 GHz–8.0 GHz Single-Chip Transceiver for MB-OFDM UWB in 0.18-μm CMOS Process," *Journal of Solid-State Circuits*, vol. 44, no. 18, pp. 414 - 426, Feb. 2009.

[9] Y. Zhao, J.-F. Frigon, K. Wu, and R.G. Bosisio, "Multi(Six)-Port Impulse Radio for Ultra-Wideband," *IEEE Trans. Microwave Theory Tech*., vol. 54, no. 4, pp. 1707 - 1712, Apr. 2006.

[10] D. Wang and S. Gong, "Introduction to the Front-End Receiver for Ultra-Wideband Applications," *Internal Report,* Aug. 2006.

[11] J. Li, R.G. Bosisio, and K. Wu, "A Six-port Direct Digital Millimetre-Wave Receiver," *IEEE MTT-S Int. Microwave Symp. Dig.,* pp. 1659 - 1662, San Diego, CA, May 1994.

[12] J. Li, R.G. Bosisio, and K. Wu, "Computer and Measurement Simulation of a New Digital Receiver Operating Directly at Millimetre-Wave Frequencies," *IEEE Trans. Microwave Theory Tech*., vol. 43, no. 12, pp. 2766 - 2772, Dec. 1995.

[13] S. O. Tatu, E. Moldovan, K. Wu, R.G. Bosisio and T. A. Dendini, "Ka-band Analog Front-End for Software-Defined Direct-Conversion Receiver," *IEEE Trans. Microwave Theory Tech*., vol. 53, no. 9, pp. 2768 - 2776, 2005.

[14] S. O. Tatu, and E. Moldovan, "V-band Multiport Heterodyne Receiver for High Speed Communication Systems," *EURASIP Journal on Wireless Communication and Networking*, vol. 2007, Article ID 34358, 2007.

[15] E. Moldovan, S. O. Tatu, and S. Affes, "A 60 GHz Multi-Port Front-End Architecture with Integrated Phased Antenna Array," *Microwave and Optical Technology Letters*, vol. 50, no. 5, pp. 1371 - 1376, 2008.

[16] E. Moldovan, S. Affes, and S. O. Tatu, "A 60 GHz Multi-Port Receiver with Analog Carrier Recovery for Ultra Wideband Wireless Personal Area Networks," *2008 European Microwave Week*, Conference proceedings, pp. 1779 - 1782, Amsterdam, 2008.

[17] D. Pozar, *Microwave Engineering*, JohnWiley & Sons, 2005.

[18] Y. Ding, and K. Wu, "Half-mode substrate integrated waveguide six-port front-end circuits for direct-conversion transceiver design," *IEEE MTT-S Int. Microwave Symp. Dig.*, pp. 1175 - 1178, San Diego, CA, Jun. 2008.

[19] S. O. Tatu, E. Moldovan, K. Wu, and R.G. Bosisio, "A New Direct Millimeter-Wave Six-Port Receiver," *IEEE Trans. Microwave Theory Tech*., vol. 49, no. 12, pp. 2517 - 2522 Dec. 2001.

[20] X. Xu, R.G. Bosisio, and K. Wu, "A New Six-Port Junction Based on Substrate Integrated Waveguide Technology," *IEEE Trans. Microwave Theory Tech*., vol. 53, no. 3, pp. 2267 -7272, Jul. 2005.

[21] E. Moldovan, S. O. Tatu, T. Gaman, K. Wu, and R.G. Bosisio, "A New 94 GHz Six-Port Collision Avoidance Radar Sensor," *IEEE Trans. Microwave Theory Tech*., vol. 52, no. 3, pp. 751 - 759, Mar. 2004.

[22] R. Ludwig and P. Bretchko, *RF Circuit Design. Theory and Applications*, Prentice Hall 2000.

[23] Y. Zhao, C. Viereck, J.F. Frigon, R.G. Bosisio, K.Wu, "Direct quadrature phase shift keying modulator using six-port technology," *Electronics Letters, v*ol. 41, Oct. 2005 pp. 1180 – 1181.

[24] S. Abielmona, H. V. Nguyen, C. Caloz, K. Wu, and R. G. Bosisio, "Compact multilayer ultra-wideband six-port device for modulation/demodulation," *Electronics Letters,* vol. 43, pp. 813 – 814, Jul. 2007.

[25] S. Gong, M. Karlsson, A. Serban, J. Östh, and O. Owais, "Radio architecture for parallel processing of extremely high speed data," *IEEE Int. Conf. on Ultra-Wideband*, ICUWB 2009, Vancouver, Canada, 2009.

[26] N. K. Mallat, S. O. Tatu, "Six-Port Receiver in Millimeter-Wave Systems," *IEEE International Conference on Systems, Man and Cybernetics*, 2007 ISIC, pp. 2693 - 2697, Oct. 2007.

[27] A. Serban, J. Östh, Owais, M. Karlsson, S. Gong, Jaap Haartsen and Peter Karlsson "Six-Port Transceiver for 6-9 GHz Ultra-Wideband Systems," *Microwave and Optical Technology Letters*, accepted paper, 2009.

[28] Adriana Serban, Joakim Östh, Owais, Magnus Karlsson, Shaofang Gong, Jaap Haartsen and Peter Karlsson, "Six-Port Direct Carrier Modulator at 7.5 GHz for Ultra-Wideband Applications," manuscript.

CHAPTER 4 SIX-PORT 6-9 GHZ TRANSCEIVERS

In this chapter, ultra-wideband 6-9 GHz receiver and transmitter front-end topologies for Gbit/s data rates and low power consumption are investigated. To capture the advantages offered by distributed passive components, both the transmitter and receiver use the six-port correlator as the core of a passive mixer. Firstly, a system level architecture is proposed for Gbit/s data rates. Using multi-level quadrature amplitude modulation (M-QAM) schemes and a top-down design methodology, the transmitter and receiver topologies are verified using simulations. Then, a new six-port modulator is proposed for M-QAM modulation. The modulator is implemented with field-effect transistors (FET). The potential but also the limitations of the FET used as controlled-impedance are presented. Finally, the feasibility of the six-port transmitter for high data rate wireless transmission is discussed. This chapter completes and reflects a part of the work which has been presented in *Paper II*, *Paper VI* and *Paper VII*.

4.1. Six-Port Transceiver Architecture for Gbit/s Data Rates

Since firstly introduced in 1994, the six-port technique has been gradually accepted as a low-power and low-cost alternative to conventional receiver topologies for radio and radar applications [1]-[7]. Some advantages of the six-port techniques were discussed in Chapter 4. Moreover, in *Paper II* [8] it is shown that extremely wideband six-port correlator can be manufactured in a low-cost printed circuit board with excellent performances in terms of amplitude and phase balance. This makes the six-port correlator particularly interesting for ultra-wideband transceiver design for high data rates

Our interest in six-port radio architecture started with ultra-wideband 3.1-4.8 GHz (UWB) radio front-end topologies for short-distance wireless communications implemented in a low-cost printed circuit board (PCB) process [5]-[7]. This frequency range corresponds to the Band Group 1 of the multi-band

orthogonal frequency-division multiplexing (MB-OFDM) specification as initially proposed by the WiMedia Alliance [9]. As shown in Chapter 1 and in *Paper II* [8], in order to avoid interference with other radio systems and due to the perspective of world-wide interoperability, the 6-9 GHz band is preferred today by the industry. Therefore, recent research activity presented in this chapter is focused on the development of 6-9 GHz transceiver for above 10 Gbit/s data rate.

4.2. Six-Port Transceiver Architecture

The possibility of high data rate transmission requires broadband communication systems. Beside wide bandwidth, high data rates can be accomplished by different approaches in terms of system architecture, modulation techniques and circuit solutions.

Compared to the previously developed 3.1-4.8 GHz six-port transmitter-receiver pair [7], the 6-9 GHz six-port transceiver requires new circuit solutions and design approaches in order to fulfil operation with around 10 Gbit/s bit rates while accommodating the newly worldwide approved 6-9 GHz UWB standard. Theoretical analysis presented in *Paper VI* [10] using Shannon's theorem [11], Friis equation [12] and UWB specifications in terms of the average EIRP (equivalent isotropic-radiated power) density of -41.3 dBm/MHz shows that a large bandwidth and a high modulation order are essential in order to achieve data rate above 10 Gbit/s in a short-range (~two meters).

To answer the high requirements on amplitude and phase balance of the quadrature LO signals as well as the requirements of low-power consumption and low noise figure, an unconventional wideband six-port transceiver architecture was proposed. The proposed 6-9 GHz six-port transceiver architecture shown in Figure 4.1 uses three parallel channels. Each channel has 1 GHz bandwidth, accordingly covering the frequency spectrum 6-7, 7-8, and 8-9 GHz. This architecture follows the more general radio architecture for parallel processing of wireless data above 10 Gbit/s described in *Paper VI* [10]. The radio architecture is dedicated to a complete integration of the UWB front-end including the UWB antenna on the same RF module. Our previous studies on the antenna-LNA integration in a multi-layer printed-circuit board presented in

Paper III and *Paper V* have confirmed both the design methodology and the importance of antenna-LNA implementation in the same substrate [13]-[14].

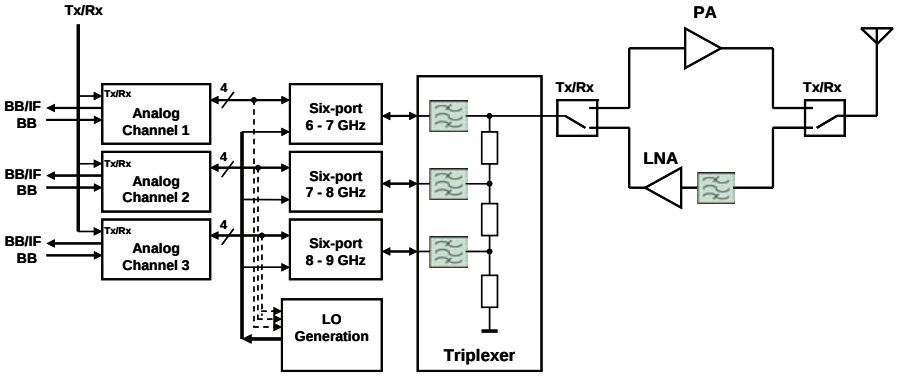

Figure 4.1. Block diagram of the six-port transceiver for Gbit/s data rate.

In Figure 4.1, the wideband transceiver includes an ultra-wideband antenna, low-noise amplifier (LNA), power amplifier (PA), two RF switches, a triplexer, three six-port correlators, and three analog channels to the baseband. A LO generation block generates three local oscillator signals (LO_i, i = 1, 2, 3).

The key components in this architecture are passive microstrip circuits, i.e., the six-port correlator and the frequency multiplexing network (FMN). The FMN ("triplexer" in Figure 4.1) is a bidirectional passive component with multiplexing/demultiplexing (mux/demux) characteristics. Introduced in [15]-[18], the proposed FMN combines a multi-band pre-selecting filter function with the frequency multiplexing function. First successful applications of the FMN technique were presented in *Paper III* and *Paper V* [13]-[14] where a new, alternative front-end for 3.1-4.8 GHz MB-OFDM operation was presented.

In the receiver RX-mode, the received modulated RF signal is automatically divided into parallel sub-channels by the FMN. The modulated signal and the corresponding LO signal are fed into the six-port circuit and after analog processing within the analog channel, the baseband signals (BB) are delivered to the output. In the transmitter (TX) mode, multi-level quadrature amplitude modulation (QAM) is achieved from the baseband binary data. The analog channel includes (a) TX/RX mode switches, (b) receiver mode decision circuits and (c) transmitter mode baseband signal controlled impedance terminations.

The proposed configuration can easily be adapted to more or less number of channels depending on the required channel capacity, available bandwidth and limitations in analog signal processing and baseband circuit limitations [10].

4.3. Six-Port Transceiver Behavioral Model

Modern design methodologies are based on early simulation on system level using behavioral models. Different blocks within the transceiver chain can have different impact on system performance. Using behavioral models, suitable circuit specifications can be determined and performance-limiting aspects can be identified. Moreover, new circuit- or system solutions can be gradually introduced, verified and compared to previous ones. Furthermore, as the design flow proceeds, behavioral models are replaced by true component and true-circuit models ensuring that the system will perform according to the specification.

Using the top-down design methodology, behavioral models of the receiver and transmitter were firstly developed using Advanced Design System (ADS) from Agilent Technologies Inc. Simulation set-ups for QPSK, 16- and 64-QAM modulation/demodulation applications of the six-port transmitter and receiver were developed in ADS Analog/RF and DSP modes. System level simulations were performed using Circuit Envelope simulator in ADS from Agilent Technologies Inc.

4.3.1. Transmitter Behavioral Model

The primary objective of the behavioral transmitter model was to generate a simulation set-up in ADS environment for further testing of new six-port modulator topologies for M-QAM modulation.

Usually, the six-port modulator presented in Chapter 3, is preferentially used in conjunction with RF switches at port 3 to 6 toggling termination impedances between two values corresponding to SHORT and OPEN [19]. However, as shown in *Paper II* [8], for a 64-QAM modulation scheme more than two controllable values of the impedance termination are required. The conceptual block diagram of a six-port modulator for M-QAM modulation is shown in Figure 4.2.

Firstly, an encoding scheme was proposed with $\Gamma_3 = \Gamma_4$ and $\Gamma_5 = \Gamma_6$. The behavioral switch models in ADS were modelled with variable internal resistance controlled by PRBS voltage sources to generate the baseband I- and Q-data. For 64-QAM modulator operation, eight impedance termination values were attributed for symmetrical distribution of the reflection coefficients between -1 and +1. Detailed information can be found in *Paper II* and *Paper VII*, [8], [21]. Simulation results shown in *Paper II* confirmed the six-port modulator model and the simulation set-up using the circuit envelope simulator.

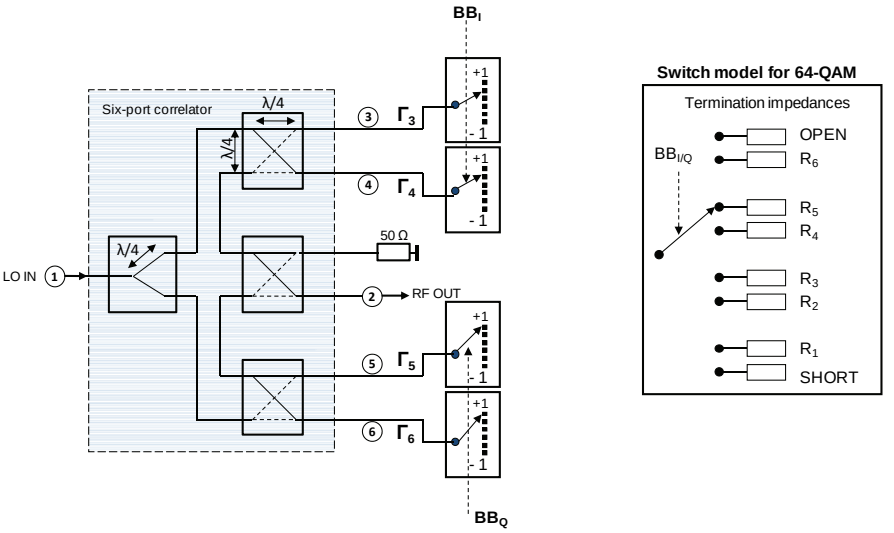

Figure 4.2 Conceptual block diagram of the six-port modulator for 64-QAM modulation.

4.3.2. Receiver Behavioral Model

The six-port direct conversion receiver shown in Figure 4.3a was modelled in ADS using behavioral models for all circuits. Simulations were done with a 64-QAM modulated RF signal with the carrier frequency f_c = 7.5 GHz. For future six-port transceiver design purposes, the heterodyne receiver was also modeled and simulations were performed. The frequency planning is similar to a classical heterodyne receiver with one IF down-conversion as shown in Chapter 3, Figure 3.6, but with a fixed LO1 frequency. Simulations were done using a 64-QAM modulated RF signal with the carrier frequency f_c = 7.5 GHz. The symbol rate was varied and the IF signal frequency was 2.5 GHz. Moreover, all the

simulations have assumed that the LO and carrier signals have the same frequency. The simplified diagrams of a heterodyne six-port receiver are shown in Figure 4.3b.

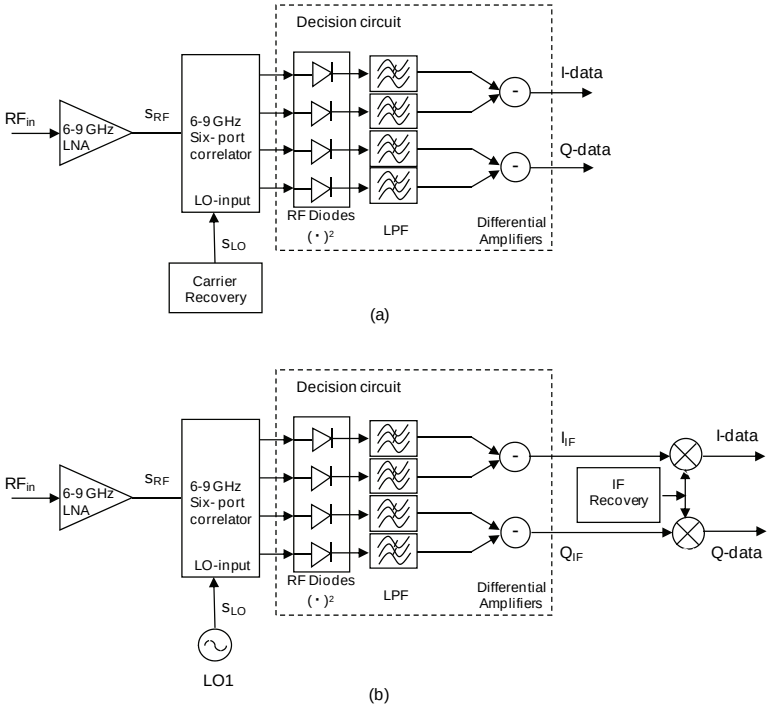

Figure 4.3. Simplified diagram of the wideband six-port receiver front-end: (a) direct-conversion topology and (b) heterodyne topology.

Simulation results using six-port modulator and receiver behavioral models are presented in *Paper II* [8] and *Paper VII* [20]. They mainly confirm the simulation set-up in ADS for different modulation schemes. More realistic simulations are done introducing true component and circuit models as presented in *Paper VII*.

4.4. Six-Port Transceiver Implementation

A 7-8 GHz six-port transmitter and receiver were designed and then separately integrated in a double-sided Rogers 4350B printed circuit board

On the receiver site, the previous 3.1-4.8 GHz receiver [5] was adapted to the 7-8 GHz UWB band operation mainly by using components of better performance. The differential amplifiers were implemented with LMH6703 operational amplifier from National Semiconductors having a 4200 V/μs slew rate. The power detectors were zero-bias Schottky diodes, BAT15-07LRH from Infineon Technology. To date, first measurement results show that demodulation of a 16-QAM signal with a data rate of 1.67 Gbit/s is possible with a bit-error rate about $4x10^{-3}$.

On the transmitter side, a six-port modulator scheme for higher order modulation than QPSK was firstly proposed. The proposed UWB six-port modulator shown in Figure 4.4 uses field-effect transistors (FET) with zero drain-source bias as controlled impedance terminations. Previous reported six-port modulators have used commercial switch matrix in conjunction with SHORT and OPEN terminations for QPSK [19] and 16-QAM [20] modulation schemes.

Design challenges of the proposed six-port modulator implemented with FETs as controlled impedance terminations for higher order modulation than QPSK were firstly identified:

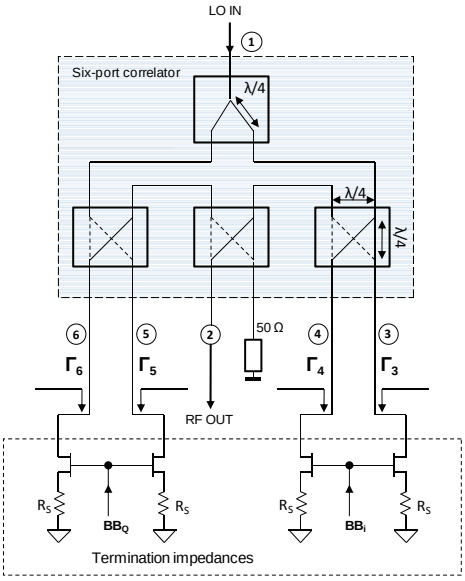

Figure 4.4. Simplified diagram of the six-port modulator with FETs as controlled impedance terminations.

- Optimal transistor topology including bias point operation selection.
- Broadband termination impedance value control.
- Limits of the modulation order due to package and transistor parasitics.

First simulations of the six-port modulator using a real component models were done using NEC NE3511 and a 7-8 GHz six-port correlator. The S-parameters of the six-port correlator were extracted using electromagnetic simulator Momentum in ADS. The design methodology of the impedance termination with true component FET include transistor S-parameter simulation for different V_{GS} values and V_{DS} = 0. Firstly, the optimal FET topology is determined, than the V_{GS} range is identified for desired reflection coefficients values with symmetrical spreading across the Smith chart. Simulation results showed that QPSK-modulated signal with symbol rates up to 1200 Mbit/s can be generated. Simulations performed with true-component models and measurement results are presented in *Paper II* [8] and *Paper VII* [21]. Spectral response measurements showed that 16-QAM modulated signals250 Msymbol/s (= 1 Gbit/s data rate) can be generated even with impedance terminations far from the ideal case. Detailed information about the six-port modulator can be found in *Paper VII*.

Finally, the 6-9 GHz UWB LNA was designed as an all-microstrip dual-section LNA topology. The layout of the LNA is shown in Figure 4.5a. To date, simulation results predict low-noise figure and relatively flat power gain, as illustrated in Figure 4.5b and 4.5c.

4.5. Six-Port Transceiver – Summary

Systems that address short-range high-data-rate wireless communication face specific challenges when integrated in CMOS processes with conventional transceiver architectures. To avoid some of them, we propose to use the six-port correlator as the core of both transmitter and receiver architectures.

Using six-port transceiver can reduce hardware complexity, power consumption and cost for wireless applications. As known, power consumption is a major engineering concern in any transceiver design aimed for wireless mobile communication. Using the six-port transceiver approach, the RF front-end

becomes not only simpler but also “passive”, with all the advantages which passive components have at high frequency when integrated as distributed components.

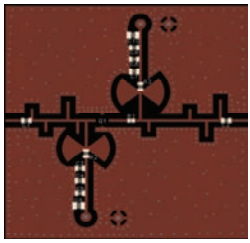

(a)

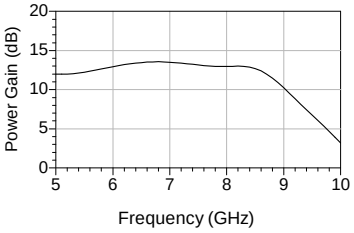

(b)

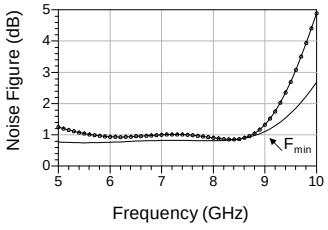

(c)

Figure 4.5. UWB LNA for 6-9 GHz: (a) layout, (b) simulated forward transmission, and (c) simulated noise figure (circle). F_{min} (solid), is minimum achievable noise figure.

Moreover, passive processing of RF signals is not only power-efficient but also results in good linearity of the overall system over a wideband, as shown in *Paper VI* [10]. Main metrics of the circuits, such as loss, noise figure, power gain are highly predictable due to accurate RF-specific simulations. They have small tolerances compared with the designed values (*Paper I*).

As shown, six-port transceivers allow transmission of complex data symbols which can belong to different modulation schemes, from QPSK to M-QAM, where verified maximum values of M in our to date measurement results is M = 64. Moreover, up- and down-conversion of frequencies is accomplished with only one phase of the LO signal, i.e., no in- and quadrature-phase LO signals are necessary.

The six-port transceiver is also ideal for research purposes. Thus, rapid manufacturing as a printed circuit board RF module result in short design-prototype cycles at relatively low-cost. New circuits can be investigated separately or in the more complex scenario of a receiver or transmitter chain. Rapid prototyping generates the necessary feedback in the design process of complex high-frequency systems.

4.6. References

[1] J. Li, R.G. Bosisio, and K. Wu, "A Six-port Direct Digital Millimetre-Wave Receiver," *IEEE MTT-S Int. Microwave Symp. Dig.*, pp. 1659 - 1662, San Diego, CA, May 1994.

[2] J. Li, R.G. Bosisio, and K. Wu, "Computer and Measurement Simulation of a New Digital Receiver Operating Directly at Millimetre-Wave Frequencies," *IEEE Trans. Microwave Theory Tech*., vol. 43, no. 12, pp. 2766 - 2772, Dec. 1995.

[3] S. O. Tatu, E. Moldovan, K. Wu, and R.G. Bosisio, "A New Direct Millimetre-Wave Six-Port Receiver," *IEEE Trans. Microwave Theory Tech*., vol. 3, no. 8, pp. 1809 - 1812, 2002.

[4] S. O. Tatu, E. Moldovan, K. Wu, R.G. Bosisio and T. A. Dendini, "Ka-band Analog Front-End for Software-Defined Direct-Conversion Receiver," *IEEE Trans. Microwave Theory Tech*., vol. 53, no. 9, pp. 2768 - 2776, 2005.

[5] D. Wang and S. Gong, "Introduction to the Front-End Receiver for Ultra-Wideband Applications," Internal Report, Aug. 2006.

[6] D. Wang, A. Huynh, P. Hakansson, L. Ming, and Shaofang Gong, "Study of Wideband Microstrip Correlator for Ultra-Wideband Communication Systems" Proceedings of *Asia-Pacific Microwave Conference APMC 2007*," pp. 1 - 4, Dec. 2007.

[7] P. Håkansson and S. Gong, "Ultra-wideband six-port transmitter and receiver pair 3.1-4.8 GHz," Proceedings of *Asia-Pacific Microwave Conference APMC 2008*," pp. 1 - 4, Dec. 2008.

[8] Adriana Serban, Joakim Östh, Owais, Magnus Karlsson, Shaofang Gong, Jaap Haartsen and Peter Karlsson, "Six-Port Transceiver for 6-9 GHz

Ultra-Wideband Systems," *Microwave and Optical Technology Letters* (accepted for publication).

[9] WiMedia white paper, WiMedia radio: Current regulatory status and respective industry positions, www.wimedia.org/en/resources/whitepapers.asp?id=res, 2009.

[10] Shaofang Gong, Magnus Karlsson, Adriana Serban, Joakim Östh, Owais, Jaap Haartsen and Peter Karlsson, "Radio Architecture for Parallel Processing of Extremely High Speed Data," *2009 IEEE International Conference on Ultra-Wideband (ICUWB)*, Vancouver, Canada. September 2009, *Paper VI.*

[11] S. Haykin, *Digital Communications*, John Wiley & Sons, Inc., ISBN-13: 978-0471629474, 1988.

[12] D.M. Pozar, *Microwave and RF Design of Wireless Systems*, Wiley, ISBN 0-471-32282-2, pp. 129, 2001.

[13] Adriana Serban, Magnus Karlsson, Shaofang Gong, "A Frequency-Triplexed RF Front-End for Ultra-Wideband Systems," *ISAST Transactions on Electronics and Signal Processing*, No. 1, Vol. 2, pp.83 - 88, 2008.

[14] Adriana Serban, Magnus Karlsson, Shaofang Gong, "All-Microstrip Design of Three Multiplexed Antennas and LNA for UWB Systems," *Asia-Pacific Microwave Conference, Dec 2006*, Yokohama, Japan, pp. 1109 – 1112, IEICE, Tokyo, Japan, December 2006.

[15] P. Håkansson, A. Huynh and S. Gong, "A study of wireless parallel data transmission of extremely high data rate up tp 6.17 Gbps per channel," Proceedings of *Asia-Pacific Microwave Conference APMC 2006,*"Yokohama, Japan, pp. 975 - 978, Dec. 2006.

[16] M. Karlsson, P. Håkansson, A. Huynh and S. Gong, "Frequency-multiplexed Inverted-F Antennas for Multi-band UWB," *IEEE Wireless and Microwave Conf.* 2006, pp. 2.1 - 2.3, 2006.

[17] M. Karlsson, and S. Gong, "A Frequency-Triplexed Inverted-F Antenna System for Multi-band UWB 3.1-4.8 GHz," *ISAST Transaction on Electronics and Signal Processing*, vol. 1, no. 1, pp. 95 - 100, 2007.

[18] M. Karlsson, P. Håkansson, and S. Gong, “A Frequency Triplexer for Ultra-Wideband Systems Utilizing Combined Broadside- and Edge-coupled Filters,” *IEEE Trans. On Advanced Packaging*, vol. 31, no. 4, pp. 794 - 801, Nov. 2008.

[19] S. Abielmona, et al, “Compact Multilayer Ultra-Wideband Six-Port Device for Modulation/Demodulation,” *Electronics Letters*, vol. 43, No. 15, Jul. 2007.

[20] B. Luo and M. Y. W. Chia, “Direct 16 QAM Modulator,” *Electronics Letters*, Vo. 44, No. 15, July 2008.

[21] Adriana Serban, Joakim Östh, Owais, Magnus Karlsson, Shaofang Gong, Jaap Haartsen and Peter Karlsson, “Six-Port Direct Carrier Modulator at 7.5 GHz for Ultra-Wideband Applications,” manuscript.

CHAPTER 5 OWN CONTRIBUTION AND FUTURE WORK

In this thesis the concept of a complete wideband six-port radio transceiver for high data rate transmission was investigated.

5.1. Own Contribution

First prototypes of the six-port transceiver including the 6-9 GHz UWB LNA were designed and to date, parts of the system were tested for the first evaluation and feedback. The six-port correlator, the LNA, the six-port modulator and six-port receiver were manufactured in a double-sided Rogers 4350B printed circuit board. A few new circuits for flexible implementation of the UWB radio have been suggested.

For low-power and wideband operation in the receiver front-end, an LNA topology with dual-section distributed matching networks was implemented. Using dual-section microstrip matching networks, low noise figure and flat power gain over a wideband, while keeping the power consumption low, have been demonstrated. Moreover, it was shown that multi-band UWB-compliant antenna-LNA system can be completely integrated on a printed circuit board. The importance of the antenna-LNA co-design for equal performance and low noise figure in all bands, while keeping good isolation between the three sub-bands, was firstly demonstrated in *Papers III* and *V*. In these papers, first applications of the frequency multiplexing network (FMN) in a front-end configuration have proved not only its operation but also opened the way towards later flexible UWB front-end topologies for above 10 Gbit/s data rates.

Theoretical analysis and experimental results have shown that high-frequency passive components are best implemented with distributed transmission lines.

Moreover, it was also shown that using microstrip matching networks in a low-cost substrate in conjunction with optimization techniques and statistical analyses can improve performance and manufacturing yield of UWB LNAs and the entire front-end. The good design approach has large potential to model the real-world LNA including high frequency component and EM coupling. This part of the work investigates several aspects LNA design for ultra-wideband systems with focus on UWB LNA design between 3.1-4.8 GHz. Details are presented in *Papers I*, *III*, *IV* and *V*.

In the later part of the thesis ultra-wideband 6-9 GHz receiver and transmitter front-end topologies for Gbit/s data rates and low power consumption have been investigated. To capture the advantages offered by distributed passive components, both the transmitter and receiver use the ultra-wideband six-port correlator as the core of a passive mixer. Modelling and design of the 6-9 GHz UWB front-end transceiver include different receiver topologies and different modulation schemes. The 7.5 GHz UWB transceiver front-end is finally implemented and evaluated. Measurement results confirm the large potential of the six-port UWB front-end to achieve multiple Gbit/s data rates.

5.2. Future Work

Antenna-LNA co-design

One of the interesting research subjects for future work refers to the antenna-LNA co-design for 6-9 GHz UWB applications. As seen in Section 2.2, one of the most important aspects of the UWB receiver performance is its noise figure. In order to achieve low noise figure, care must be taken in an UWB receiver design process to insure that proper impedance matching conditions are met. Any loss that occurs before the LNA in the system will substantially degrade the system overall noise performance. In order to circumvent the losses, the antenna should be closely integrated with the LNA, preferably on the same PCB. The minimum noise figure is obtained by properly selecting the matching network that transforms the impedance of the antenna to the impedance needed for low noise figure. Using the scattering (S-) parameters obtained through either full wave EM simulations or measurements of the antenna prototype, the matching network for the minimum noise can be designed and optimized. As the antenna performance can be affected by the layout environment close to it, the whole

front-end performance should be optimized over a wide frequency band using EM simulations.

Antenna-Switch-LNA and PA (Buffer) co-design

Miniaturization of the proposed six-port transceiver module is a critical factor for successful future designs. The main challenge is to integrate the entire UWB radio in a multi-layer substrate as a SiP. Problems such as transmitter-receiver isolation might appear. They are best solved if the entire front-end is optimized using a top-down design methodology, ending on the true-circuit and accurate component models level and with a realistic description of the multi-layer substrate. Powerful EDA tools and careful modelling of the entire TX/RX front-end are necessary for system optimization by co-design of the RF front-end.

Integration of the six-port transceiver in a multi-layer SiP module

Commercially available six-port transceivers for high-data-rate within the frame of the UWB regulations are a challenging task. Some of the future directions to be followed are:

Determination of the system specification and circuit specification by using a bidirectional design approach. Top-down simulations followed by bottom-up simulations with real models of the components and communication channel. The RF/digital interface specifications as well as frequency plan along the transmitter/receiver chain.

Miniaturization of the six-port transceiver is an important aspect, as the challenge is to obtain a compact and integrated design in an affordable technology which is not either traditional CMOS IC technology or MMIC technology. The main direction is a microstrip, multi-layer SiP technology [1]-[2].

Optimization of proposed six-port topology transmitter for higher data rates. More appropriate small parasitic dual-package matched transistors should be used for better performance of the modulator.

The Moore's law of CMOS scaling is now nearing its physical limits while never being actual for RF CMOS system integration. Today it is accepted that further growth of industry must be governed by "More than Moore" law [2]. This is the new motto of our time, saying that tighter integration of all modern

electronic systems and particularly integration of RF systems for wireless high-data-rate transmission can be achieved through integration at package level. System-in-Package technologies are now opening a door for new electronic system solutions with better performance and better passive components – still important at RF - while being an equal partner to System-on-Chip technologies.

5.3. References

[1] R. Ulrich, L.Schaper, “Putting passives in their place,” *IEEE Spectrum*, vol. 40, Jul. 2003, pp. 26 – 30.

[2] “The next Step in Assembly and Packaging: System Level Integration in the package (SiP),” white paper at http://www.itrs.net/papers.html, 2009.